

1 **Variation in CO<sub>2</sub> and CH<sub>4</sub> Fluxes Among Land Cover Types in Heterogeneous Arctic Tundra**  
2 **in Northeastern Siberia**

3

4 Sari Juutinen<sup>1,2</sup>, Mika Aurela<sup>1</sup>, Juha-Pekka Tuovinen<sup>1</sup>, Viktor Ivakhov<sup>3</sup>, Maiju Linkosalmi<sup>1</sup>, Aleksii  
5 Räsänen<sup>4,5</sup>, Tarmo Virtanen<sup>4</sup>, Juha Mikola<sup>4,5</sup>, Johanna Nyman<sup>1</sup>, Emmi Vähä<sup>1</sup>, Marina Loskutova<sup>6</sup>,  
6 Alexander Makshtas<sup>6</sup>, and Tuomas Laurila<sup>1</sup>

7 1) Finnish Meteorological Institute, [Climate System Research](#), Erik Palménin aukio 1, 00560  
8 Helsinki, Finland

9 2) Department of Geographical and Historical Studies, University of Eastern Finland,  
10 Yliopistokatu 2, FI-80100 Joensuu, Finland (P.O. Box 111, FI-80101 Joensuu, Finland)

11 3) Voeikov Main Geophysical Observatory, Ulitsa Karbysheva, 7, St Petersburg, 194021,  
12 Russia

13 4) Ecosystems and Environment Research Programme, University of Helsinki, Viikinkaari 1,  
14 00790 Helsinki, Finland

15 5) Natural Resources Institute Finland (LUKE), Latokartanonkaari 9,  
16 00790 Helsinki, Finland

17 6) Arctic and Antarctic Research Institute, Bering str., 38, St Petersburg, 199397, Russia

18

19

20 Corresponding author Sari Juutinen, sari.juutinen@uef.fi

21

22

23

24

25

26

27 **Abstract**

28 Arctic tundra is facing unprecedented warming, resulting in shifts in the vegetation, thaw regimes,  
29 and potentially in the ecosystem-atmosphere exchange of carbon (C). The estimates of regional  
30 carbon dioxide (CO<sub>2</sub>) and methane (CH<sub>4</sub>) budgets, however, are highly uncertain. We measured  
31 CO<sub>2</sub> and CH<sub>4</sub> fluxes, vegetation composition and leaf area index (LAI), thaw depth, and soil  
32 wetness in Tiksi (71° N, 128° E), a heterogeneous site located within the prostrate dwarf-shrub  
33 tundra zone in northeastern Siberia. Using the closed chamber method, we determined net  
34 ecosystem exchange (NEE) of CO<sub>2</sub>, dark ecosystem respiration (ER), ecosystem gross  
35 photosynthesis (Pg), and CH<sub>4</sub> fluxes during the growing season. We applied a previously developed  
36 high-spatial-resolution land-cover map over an area of 35.8 km<sup>2</sup> for spatial extrapolation. Among  
37 the land-cover types varying from barren to dwarf-shrub tundra and tundra wetlands, the NEE and  
38 Pg at light level 800 μmol m<sup>-2</sup>h<sup>-1</sup> (NEE<sub>800</sub> and Pg<sub>800</sub>) were greatest in the graminoid-dominated  
39 habitats, i.e., stream side meadow and fens with NEE<sub>800</sub> up to -21 (uptake) and Pg<sub>800</sub> up to 28 mmol  
40 m<sup>-2</sup> h<sup>-1</sup>. Vascular LAI was a robust predictor of a NEE<sub>800</sub> and Pg<sub>800</sub> and, on a landscape scale, the  
41 fens were disproportionally important for the summertime CO<sub>2</sub> sequestration. Dry tundra, including  
42 the dwarf-shrub-dominated vegetation and and barren, had smaller CO<sub>2</sub> exchange rates. The fens  
43 were dominant source of CH<sub>4</sub>, while the dry mineral soil tundra consumed atmospheric CH<sub>4</sub>, which  
44 on a landscape scale was -9 % of the total CH<sub>4</sub> balance. The largest seasonal mean CH<sub>4</sub>  
45 consumption rate of 0.02 mmol m<sup>-2</sup> h<sup>-1</sup> occurred in barren with sand and stone cover. The high  
46 consumption value agrees well with the consumption estimate based on eddy covariance  
47 measurements from the same site. We acknowledge the uncertainty involved in spatial  
48 extrapolations due to a small number of replicates per land-cover type. This study, however,  
49 highlights the need for distinguishing different land-cover types including the dry tundra habitats to  
50 account for their CO<sub>2</sub> and CH<sub>4</sub> flux patterns, including the consumption of atmospheric CH<sub>4</sub>, when  
51 estimating tundra C exchange on a larger spatial scale.

## 52 **1 Introduction**

53 It is uncertain whether the Arctic tundra is a sink or a source of atmospheric carbon (C). The current  
54 estimates suggest a sink of 13–110 Tg C yr<sup>-1</sup>, but their uncertainty range crosses the zero balance  
55 (McGuire et al. 2012, Virkkala et al. 2020). Improving these estimates is vital, because the Arctic  
56 tundra covers a vast area of 7.6 million km<sup>2</sup> (Walker 2000) that is experiencing substantial warming  
57 (IPCC 2013, Chen et al. 2021). Warming can alter C exchange and, either amplifying or mitigating  
58 mitigate climate change through ecosystem–atmosphere interactions. Some local-scale studies  
59 suggest that the Arctic tundra is shifting from a small sink to a source of C (Webb et al. 2016,  
60 Euskirchen et al. 2017). It is likely that the climate change response of the ecosystem carbon  
61 dioxide (CO<sub>2</sub>) sink strength and methane (CH<sub>4</sub>) emissions, whether an increase or a decrease,  
62 depends on site-specific changes in thawing, wetness, temperature, and vegetation (McGuire et al.  
63 2018). ~~C-Dynamics of C exchange different tundra habitats~~ need to be quantified across the Arctic  
64 habitats to improve the upscaling of arctic CO<sub>2</sub> and CH<sub>4</sub> balances and to monitor how ecosystems  
65 respond to environmental changes.

66           The uncertainty in the arctic C balance estimates arises from the sparse and uneven  
67 observation network, which provides poor support for model-based spatial extrapolation (*cf.*  
68 McGuire et al. 2018, Virkkala et al. 2021, Kuhn et al. 2021). On a local scale, landscape  
69 heterogeneity and the related difficulty of mapping the spatial distribution of habitats and their C  
70 fluxes add to this uncertainty (McGuire et al. 2012, Treat et al. 2018, Saunois et al. 2020). In  
71 addition, year-to-year variations in seasonal features, particularly the timing of spring, summer  
72 temperatures, and snow depth have been found to cause substantial variation in the annual net CO<sub>2</sub>  
73 and CH<sub>4</sub> balances (Aurela et al. 2004, Humphreys and Lafleur 2011, Zhang et al. 2019). Fine-scale  
74 spatial heterogeneity in soil water saturation, thaw depth, vegetation characteristics, and soil organic  
75 content is typical of the tundra landscape (*e.g.*, Virtanen and Ek 2014, Mikola et al. 2018, Lara et al.  
76 2020). These factors control CO<sub>2</sub> and CH<sub>4</sub> exchange, and on an annual scale, tundra wetlands

77 typically act as net CO<sub>2</sub> sinks while upland tundra areas have a close-to-neutral C balance (*e.g.*,  
78 Marushchak et al. 2013, Virkkala et al. 2021). While tundra wetlands are substantial sources of  
79 CH<sub>4</sub>, dry tundra acts as a small-sink or small source of atmospheric CH<sub>4</sub> ([Bartlett and Harriss 1993](#),  
80 [Kuhn et al. 2021](#)). ~~A rshowed that theof dry tundra e.~~  
81 Mineral soil tundra barrens, however, have been ~~found~~identified to have high  
82 consumption rates of atmospheric CH<sub>4</sub>, which is due to the high-affinity methane oxidizing bacteria  
83 ([Emmertson et al. 2014](#), [Jørgensen et al. 2014](#), [D’Imperio et al. 2017](#), [Oh et al. 2020](#)). These bacteria  
84 can utilize atmospheric CH<sub>4</sub> as energy source at low atmospheric concentrations, opposite to the  
85 low-affinity methane oxidizers that require higher CH<sub>4</sub> concentrations and occur in wetlands (*e.g.*,  
86 [Oh et al. 2020](#)). A modeling exercise that ~~introduced~~accounting the high-affinity methanotrophy for  
87 mineral-rich soils resulted in a doubling of the circumpolar soil CH<sub>4</sub> sink above 50° N compared to  
88 previous estimates ([Oh et al. 2020](#)). ~~Particularly, the tundra barrens show high consumption rates of~~  
89 ~~atmospheric CH<sub>4</sub> due to the high-affinity methane oxidizing bacteria ([Jørgensen et al. 2014](#), [Lau et](#)~~  
90 ~~[al. 2015](#), [D’Imperio et al. 2017](#), [Oh et al. 2020](#)).~~ Thus, distinguishing dry and wet tundra with their  
91 moisture and vegetation characteristics is crucial when mapping C exchange within the tundra  
92 biome. [Treat et al. \(2018\)](#) tested spatial resolution requirements for such mapping on a landscape  
93 level and found that a 20-m pixel size captured the spatial variation in a reasonable manner, while a  
94 coarser resolution resulted in underestimation of both the landscape-scale CO<sub>2</sub> uptake and CH<sub>4</sub>  
95 emissions. In addition, understanding the spatial heterogeneity of ecosystem C exchange  
96 substantially improves analyses of eddy covariance (EC) measurements that, while in principle  
97 representing spatially integrated fluxes, may provide biased gas flux balances in a highly  
98 heterogeneous source/sink environment, as the spatial integration of EC involves non-uniform  
99 weighting of the surface elements that contribute to the measured flux ([Tuovinen et al. 2019](#)).

100

101 The aim of this study was to assess the spatial patterns and magnitudes of CO<sub>2</sub> and  
102 CH<sub>4</sub> fluxes within heterogenous prostrate dwarf-shrub tundra in Tiksi, located in northeastern  
103 Russia. Growing season fluxes of CO<sub>2</sub> (ecosystem net exchange, photosynthesis, and respiration)  
104 and CH<sub>4</sub> were determined using the chamber method to answer the questions: (i) what is the  
105 magnitude of these fluxes in different land-cover types? ~~A~~ and (ii) how do they depend on  
106 vegetation characteristics and soil wetness? In addition, ~~to test the spatial representativeness of the~~  
107 ~~chamber data,~~ we extrapolated the ~~habitatplot~~-level measurements in space ~~and to compared~~ them  
108 with the ecosystem-level data measured with the ~~micrometeorological eddy covariance (EC)~~  
109 technique.

110

## 111 2 Materials and Methods

### 112 2.1 Study site

113 The study site is located near the Tiksi Observatory (~~see Uttal et al. 2016~~) in Sakha (Yakutia) (~~see~~  
114 Uttal et al. 2016), northeastern Russia (71.5943° N, 128.8878° E), 500 m inland off the Laptev Sea  
115 coast and, on average, 7 m above sea level (Fig. 1a). The area belongs to the middle-arctic prostrate  
116 dwarf-shrub tundra subzone (Walker, 2000) and has continuous permafrost. In the end of the  
117 growing season, the maximum thaw depth is ca. 40 cm (Mikola et al. 2018). The climate in Tiksi  
118 is defined by cold winters and cool summers. The long-term mean annual temperature and mean  
119 annual precipitation were -12.7 °C and 232 mm, respectively, during the climate-normal period  
120 1981–2010. Growing season lasts about 3 months, and the soils typically freeze in the end of  
121 September and the permanent snow falls in October and thaws in June (AARI 2018).

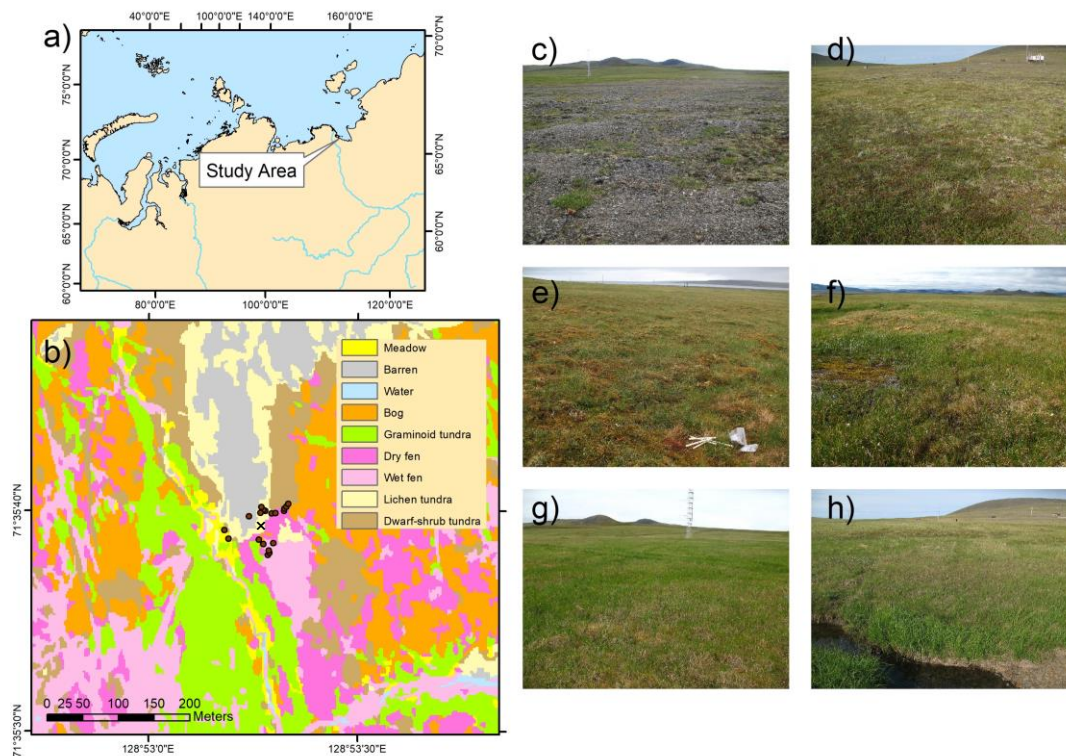
122 ~~Soil organic content varies from negligible in lichen covered and bare graveled areas~~  
123 ~~to ca. 40% in tundra wetlands (Mikola et al. 2018).~~ Bedrock ~~and soils are~~ alkaline, resulting in  
124 high plant species richness. Vegetation consists of mosses, lichens, grasses, sedges, prostrate dwarf-  
125 shrubs such as willows (*Salix* spp.), dwarf birch (*Betula nana*), and *Diapensia lapponica*, and forb

126 species (~~Fig. 1,~~ Table 1). The average heights of dwarf-shrub species are 4–6 cm and the leaf area  
127 index (LAI) of vascular plants reaches up to 1 m<sup>2</sup> m<sup>-2</sup> in the wetland fen and meadow habitats with  
128 graminoid vegetation (Juutinen et al. 2017). The land cover at the site has been classified *a priori*  
129 and mapped based on a combination of field inventories and high-spatial resolution satellite images  
130 (Mikola et al. 2018). The *a priori* land-cover types (LCT) consist of wet fen, dry fen, graminoid  
131 tundra, bog, meadow at the stream bank, dwarf-shrub tundra, and lichen tundra that consists of  
132 ~~(includes barren ground with rocks and sand and patches of vegetation ground with vegetation~~  
133 ~~patches)~~ (Table 1, Fig. 1 c–h, for a closer view see Fig. A1A). Organic layer depth is negligible in  
134 lichen tundra and a few centimeters in dwarf-shrub tundra, meadow, and graminoid tundra. In the  
135 bog, dry fen, and wet fen, the organic layer depth is~~was~~ at least the maximum depth of the active  
136 layer, i.e. ca. 30–40 cm. Soil organic content varies from negligible in lichen tundra and barren to  
137 ca. 40 % in tundra wetlands (Mikola et al. 2018).– A section of the wet and dry fen within the EC  
138 footprint area is disturbed by vehicle tracks that create open water surfaces, and there is also an area  
139 of eroded bare-peat surface on a dry fen.

140

141

142



143

144 **Fig. 1. a)** Location of the study area in Tiksi, Yakutia, Russia, **b)** Land-cover map with the and the  
 145 chamber flux measurement points (dots) and the EC mast (x)-on-the-map, and photos of the LC  
 146 types: **c)** lichen tundra with barrens, lichens, and patches of vegetation, **d)** dwarf-shrub tundra, **e)**  
 147 bog, **f)** wet and dry fen, **g)** graminoid tundra, and **h)** meadow by the stream. See Tuovinen et al.  
 148 (2019) for the EC footprint climatology.

149

150

151

152

153

154

155

156

157

158

159



160 **Table 1.** Soil and vegetation characteristics of the land cover types (LCT) and their proportions in  
 161 the EC impact area (90% of the cumulative footprint).

LCT	Soil properties and plant taxa	Proportion (%) <sup>2</sup>
Lichen tundra <sup>1</sup>	Mixture of vegetated patches, stones, and bare ground. <i>Lichens, e.g. genera Thamnolia, Flavocetraria, Alectoria, Stereocaulon, dwarf shrubs Dryas octopetala, Vaccinium vitis-idaea, Salix polaris, Diapensia lapponica, and forbs Oxytropis spp, Astragalus spp., Pedicularis spp., Artemisia spp., Minuartia sp.,</i>	8 (barren), <u>11 sparse vegetation</u>  <del>11 (sparse vegetation)</del>
Dwarf-shrub tundra	Shallow organic layer on mineral soil ground Feather mosses, lichens, <i>Salix polaris, Vaccinium vitis-idaea, Vaccinium uliginosum, Dryas octopetala, Cassiope tetragona, Betula nana, Polygonum viviparum, Pedicularis spp., Carex spp.</i>	18
Meadow	Shallow organic layer on mineral soil ground <i>Calamagrostis sp., Festuca sp, Salix spp. Polygonum viviparum, Bistorta major, Polemonium sp., Valeriana sp.</i>	1.4
Graminoid tundra	Shallow peat layer on mineral soil ground Feather mosses, <i>Sphagnum spp., Carex spp., Eriophorum spp., Calamagrostis spp., Salix spp., B. nana, Saxifraga spp., Ranunculus spp., Bistorta major, Stellaria sp., Valeriana sp., Polemonium sp., Comarum palustre</i>	13
Bog	Dry hummock habitat at the tundra peatland <i>Sphagnum spp., feather mosses, Salix spp., Vaccinium uliginosum, Vaccinium vitis-idaea, Betula nana, Rhodendron tomentosum, Cassiope tetragona, Carex spp., Polygonum viviparum., Stellaria sp.</i>	23
Dry fen	Intermediate wet tundra peatland habitat <i>Sphagnum spp., Carex spp., Salix spp, Saxifraga spp., Comarum palustre, Epilobium spp., Ranunculus spp., Pedicularis spp., Stellaria sp.</i>	10
Wet fen	Wet tundra peatland habitat with open pools <i>Brown mosses, Carex spp., Eriophorum spp., Ranunculus sp., Caltha palustris, Pedicularis sp., Saxifraga sp.</i>	15

162 <sup>1)</sup> Combined land-cover types bare and lichen tundra in Juutinen et al. (2017), Mikola et al. (2018),  
 163 Tuovinen et al. (2019), <sup>2)</sup> Proportion within the 90% coverage of the mean EC footprint area during  
 164 the growing season of 2014 (Tuovinen et al. 2019).

165

166



167 2.2 CO<sub>2</sub> and CH<sub>4</sub> flux measurements

168 Fluxes of CO<sub>2</sub> and CH<sub>4</sub> were measured using static chambers [equipped with a fan and](#) set on ~~12~~-pre-  
 169 installed collars of 50 cm × 50 cm. The measurement points (collars) were set to cover the  
 170 heterogeneity in land cover, and in each study year, there were 1–4 measurement points per each  
 171 LCT (Table 2). Most of the data were collected during a study campaign in July 15 – August 16,  
 172 2014 ([12 collars](#)). The growing season had started earlier due to a warm period and daily mean air  
 173 temperature stayed over 5 °C since July 5 (Fig. 2) (Tuovinen et al. 2019). Net ecosystem exchange  
 174 of CO<sub>2</sub> (NEE) and ecosystem respiration of CO<sub>2</sub> in dark (ER) were measured using transparent and  
 175 opaque chambers (transparent chamber covered with a hood), respectively, allowing the [partitioning](#)  
 176 ~~of estimation of~~ ecosystem gross photosynthesis (Pg) ~~as difference of NEE~~ and ER. Fluxes of CH<sub>4</sub>  
 177 were determined from closures of both transparent and opaque chambers, but because there was no  
 178 difference between them when performed consecutively, the data from ~~transparent-opaque~~ chamber  
 179 measurements were used for flux calculations. In addition, CH<sub>4</sub> fluxes were measured during  
 180 shorter campaigns in 2012, 2013, 2016, and 2019 (Table 2). These data also included vehicle track  
 181 disturbance plots and an eroded bare-peat surface, which were measured in 2019.

182 **Table 2.** Measurement periods, measured fluxes (CH<sub>4</sub>, ER, NEE), and number of measurement  
 183 points and observations (points, observations) in each land cover type (LCT) across the study years.

LCT	2012	2013	2014	2016	2019
	Jul 18–21	Jul 5–Sep 3	Jul 15–Aug 16	May 30, Aug 4–5, Sep 13–14	Aug 28–Sep 1
	CH <sub>4</sub>	CH <sub>4</sub>	ER, NEE, CH <sub>4</sub>	CH <sub>4</sub>	CH <sub>4</sub>
Wet fen	4, 4	6, 22	3, 107	3, 27	5, 72
Vehicle track					2, 30
Dry fen	2, 2	4, 11	3, 107	3, 14	2, 26
Bare peat					1, 15
Bog	2, 2	3, 7	1, 36		1, 13
Meadow	1, 1	2, 6	2, 62		
Dwarf-shrub tundra	1, 1		1, 36	1, 1	
Lichen tundra		1, 3	2, 67	2, 18	2, 29
Snow and ice <sup>1</sup>				2, 2	

<sup>1</sup>Measured only on May 30, 2016.

184 In 2012 and 2013, four air samples were taken from the chambers using syringes. The  
185 samples were stored in glass vials prior the analysis. First, a vial was flushed with the sample and  
186 then filled to over-pressure. The samples were analyzed for CH<sub>4</sub> concentration using a TSVET 500-  
187 M gas chromatograph (Chromatek, Ru) with a flame ionization detector at the laboratory of the  
188 Voeikov Main Geophysical Observatory within a month from sampling. Each measurement was  
189 accompanied by calibration using standard gas mixtures with the NOAA2004 scale. The vials were  
190 tested prior to the field sampling using a standad gas: after two weeks, the vials were still over-  
191 pressurized and sample CH<sub>4</sub> concentrations were within ±3 ppb of the initial standard gas  
192 concentration ~~CH<sub>4</sub> concentrations inside the chamber were analyzed from samples stored in glass~~  
193 ~~vials using a gas chromatograph equipped with a flame ionization detector in the laboratory of the~~  
194 ~~Voeikov Main Geophysical Observatory. Four samples per each 20 min chamber closure were~~  
195 ~~collected.~~ Since July 2014, CH<sub>4</sub> and CO<sub>2</sub> concentrations inside the chambers were recorded every  
196 second during closures of about 5 min using a gas analyzer (DLT-100, Los Gatos Research, Inc.,  
197 San Jose, CA, USA) ~~DLT-100~~ (~~see appendix #~~Fig. A2 for examples). Gas fluxes between the  
198 ecosystem and the atmosphere were calculated from the phase of linear concentration change in the  
199 chamber head space over time accounting for temperature, volume, and atmospheric pressure.  
200 Concentration change during each chamber closure was evaluated visually for determining the  
201 closure start time and to remove cases showing nonlinearity due to leaks, ebullition, or saturation.  
202 The first data points were generally neglected when determining the slope of concentration change  
203 over time and cases with linear concentration change had coefficient of determination (R<sup>2</sup>) > 0.9.  
204 No change in concentration meant zero flux. There were a few ebullition cases at the vehicle track  
205 measurement points that had only sparse or no vegetation cover. When determining NEE fluxes  
206 measured using the transparent chamber, the data were screened for variation in PPFD, and rejected  
207 if the variation exceeded 100 μmol m<sup>-2</sup> s<sup>-1</sup> during the measurement.

208 The fluxes of CO<sub>2</sub> and CH<sub>4</sub> were also measured by the micrometeorological EC  
209 method, which provides continuous data of the atmosphere-biosphere fluxes averaged on an  
210 ecosystem scale. The EC system consisted of a three-dimensional sonic anemometer (USA-1,  
211 METEK GmbH, Elmshorn, Germany), a closed-path CH<sub>4</sub> analyzer (RMT-200, Los Gatos  
212 Research, Inc., San Jose, CA, USA), and a closed-path CO<sub>2</sub>/H<sub>2</sub>O analyzer (LI-COR LI-7000, LI-  
213 COR, Inc., Lincoln, NE, USA). The fluxes were calculated as 30-min averages and processed using  
214 standard methods (Aubinet et al. 2012). The EC measurement system and the post-processing  
215 procedures have been presented in more detail by Tuovinen et al. (2019).

216 Supporting meteorological measurements including air temperature (T<sub>air</sub>) (HMP,  
217 Vaisala, HMP), soil temperature (T<sub>soil</sub>) (IKES, Nokeval), photosynthetic photon flux density  
218 (PPFD) (PQS1, Kipp & Zonen, PQS1), and water table level relative to the ground surface (WT)  
219 (8438.66.2646, Trafag) were collected by a Vaisala QML datalogger as 30-min averages. We also  
220 present meteorological data for the period 2011–2019 to relate the conditions during the  
221 measurement campaign in July 15 - August 16, 2014, and the CH<sub>4</sub> flux campaigns in 2012, 2013,  
222 2014, 2016, and 2019, to longer-term variations~~the nine-year overall~~.

223

### 224 2.3 Vegetation and Topographic Wetness Index

225 On a site level, vegetation and soil characteristics were inventoried in plots assigned into a  
226 systematic grid outside the area covered by the gas flux measurement points in 2014 (see Juutinen  
227 et al. 2017; Mikola et al. 2018). The projection cover (%) of plant species and species groups, and  
228 the mean canopy height of each species group were recorded. Seven species groups were included  
229 in the inventory: *Sphagnum* mosses, feather mosses, brown mosses, dwarf shrubs, *Betula nana*,  
230 *Salix* species, forbs, and graminoids. A subset of the plots was harvested, and vascular plant leaves  
231 were scanned to determine the one-sided LAI to estimate empirical relationships between LAI and  
232 %-cover and canopy height to estimate LAI in the collars (see Juutinen et al. 2017). In the collars,

233 cover (%) and height (cm) of each species group were recorded weekly during the gas flux  
234 measurement campaign in July 15–August 16, 2014. Because there were no observational  
235 vegetation data for the other years than 2014, the green chromatic coordinate (GCC) was used as a  
236 proxy for the amount of green above-ground vascular plants (*e.g.* Richardson 2019). GCC was  
237 calculated from the digital numbers of red (R), green (G), and blue (B) color channels as the  
238 proportionratio of green in the RGB images ( $GCC = G / (R + G + B)$ ) ~~from digital RGB photos~~ of the  
239 vegetation inside the collars. The photos were taken at the time of measurements. We determined an  
240 empirical relationship between LAI and GCC by using a data set of harvested plots with digital  
241 RGB photographs and measured LAI data (n=91). For the LAI estimation, we used a linear  
242 relationship ( $R^2 = 0.46$ ,  $p < 0.001$ ) between LAI and GCC determined using the entire data set (see  
243 appendix Fig. 1-A3 for the data and equation).

244 To quantify potential soil wetness at each measurement point, we calculated the mean  
245 topographic wetness index (TWI) value based on a 2 m spatial resolution digital elevation model  
246 (Mikola et al. 2018). To characterize differences between growing seasons as manifested by  
247 vegetation greenness, MODIS Normalized Difference Vegetation Index (NDVI) with 16-day  
248 temporal and 500 m spatial resolution was calculated for a circular area with a 300 m radius from  
249 the flux tower using Google Earth Engine (Gorelick et al. 2017). NDVI was derived for 2011–2019  
250 to place the measurement years in the context of year-to-year variation in weather.

251

## 252 2.4 Data analyses

253 When examining the role of the habitat-LCT types in CO<sub>2</sub> and CH<sub>4</sub> exchange, we applied the land  
254 cover classification presented in Mikola et al. (2018). The data collected in July 15 – August 16,  
255 2014 were used for examining gas exchange in relation to the variation in LAI, GCC, WT, and TWI  
256 among the collars. The light-normalized ~~In order to estimate~~ P<sub>g</sub> and NEE at PPFD = level 800 μmol  
257 m<sup>-2</sup> s<sup>-1</sup> (P<sub>g800</sub> and NEE<sub>800</sub>, respectively), were estimated by fitting ~~a~~ a hyperbolic response function

258 ~~of CO<sub>2</sub> vs PPF~~ utilizing ~~Utilizing the~~ ER and NEE flux ~~data es measured with opaque and~~  
259 ~~transparent chambers, respectively, we assessed the light response of Pg and NEE with a hyperbolic~~  
260 ~~function~~

261

262  $NEE = ER - P_{g_{max}} \times PPF / (\beta + PPF),$  eq. (1)

263

264

265 where  $P_{g_{max}}$  is the asymptotic maximum of photosynthesis, and  $\beta$  is the half-saturation PPF. ~~To~~

266 ~~ensure comparability between different measurement days in relatively low light conditions, we~~

267 ~~determined t~~ ~~The light-normalized estimates of  $P_{g_{800}}$  and  $NEE_{800}$ , i.e.,  $P_g$  at  $PPFD = 800 \mu mol m^{-2} s^{-1}$~~

268 ~~were then calculated using the equation. The corresponding NEE, i.e.,  $NEE_{800}$ , is then obtained as~~

269 ~~a sum of  $P_{g_{800}}$  and ER.~~ Fluxes of CH<sub>4</sub> are expressed as temporally averaged per each collar

270 means. We used a sign convention where a positive value means net release to the atmosphere and a

271 negative value denotes net uptake by the ecosystem. Fluxes of CH<sub>4</sub> measured over all study years,

272 2012–2019, were averaged for each by LCT.

273

Regression analyses were used to test the relationships between gas flux estimates and  
274 vascular LAI, GCC, WT, and TWI. All CH<sub>4</sub> flux data from the years 2012–14, 2016, and 2019 were

275 used to quantify the mean growing season CH<sub>4</sub> flux for each LCT and examine the relationship

276 between CH<sub>4</sub> and GCC and TWI. To find the main factors and gradients in the plant community,

277 gas flux, and environmental variables data measured in the flux collars in 2014, we performed a

278 detrended correspondence analysis (DCA) of the species group data with post-hoc fit of

279 environmental variables, including gas fluxes, WT, LAI, GCC, elevation, and thaw depth as

280 supplementary variables. The DCA was performed on logarithmically transformed, centered species

281 data (species as species groups) using Canoco 5 (Ter Braak and Šmilauer 2012).

282

We compared the LCT-specific flux estimates based on the chamber measurements

283 with the estimates based on EC measurements over the same period. Partitioning of the EC-based

284 CO<sub>2</sub> fluxes to  $P_g$  and ER and estimates of  $P_{g_{800}}$  and  $NEE_{800}$  were calculated similarly to that of

285 chamber data using Eq. (1). The EC flux data were classified into five wind sectors (30–125°, 125–  
286 185°, 185–239°, 239–310°, 310–360°) based on the mean EC flux footprint, modeled for the  
287 growing of 2014 by Tuovinen et al. (2019). The sectors distinguished areas dominated by different  
288 LCTs, especially tundra heaths and wetlands, and, similarly, ~~those sectors~~ with a large and small  
289 vascular LAI. For each sector, the footprint-weighted areal proportions of LCTs and mean vascular  
290 LAI were derived from the high spatial resolution ~~land cover~~LCT and LAI maps (Mikola et al.  
291 2018). For this comparison, sector averages of  $P_{g800}$ , ER,  $NEE_{800}$ , and  $CH_4$  flux were calculated  
292 from the chamber data by weighting the LCT-specific flux estimates with the above-mentioned  
293 LCT proportions in each sector. Because there were no measurement points within graminoid  
294 tundra, we applied wet fen (for  $CO_2$ ) and dry fen (for  $CH_4$ ) flux estimates for the graminoid tundra  
295 based on the observed similarities in LAI and soil wetness, respectively. Overall, graminoid tundra  
296 can be considered part of the fen continuum in terms of soil characteristics (high organic content)  
297 and  $CH_4$  exchange (Mikola et al. 2018, Tuovinen et al. 2019).

298 Finally, to synthesize the  $CO_2$  and  $CH_4$  exchange variability across the tundra, we  
299 upscaled the LCT-specific average  $NEE_{800}$ ,  $P_{g800}$ , ER, and  $CH_4$  flux (2014 data) to the 35.8 km<sup>2</sup> area  
300 surrounding our study site, for which a LCT map was produced by Mikola et al. (2018).

301

## 302 **3 Results**

### 303 *3.1 ~~Meteorology~~Environmental conditions*

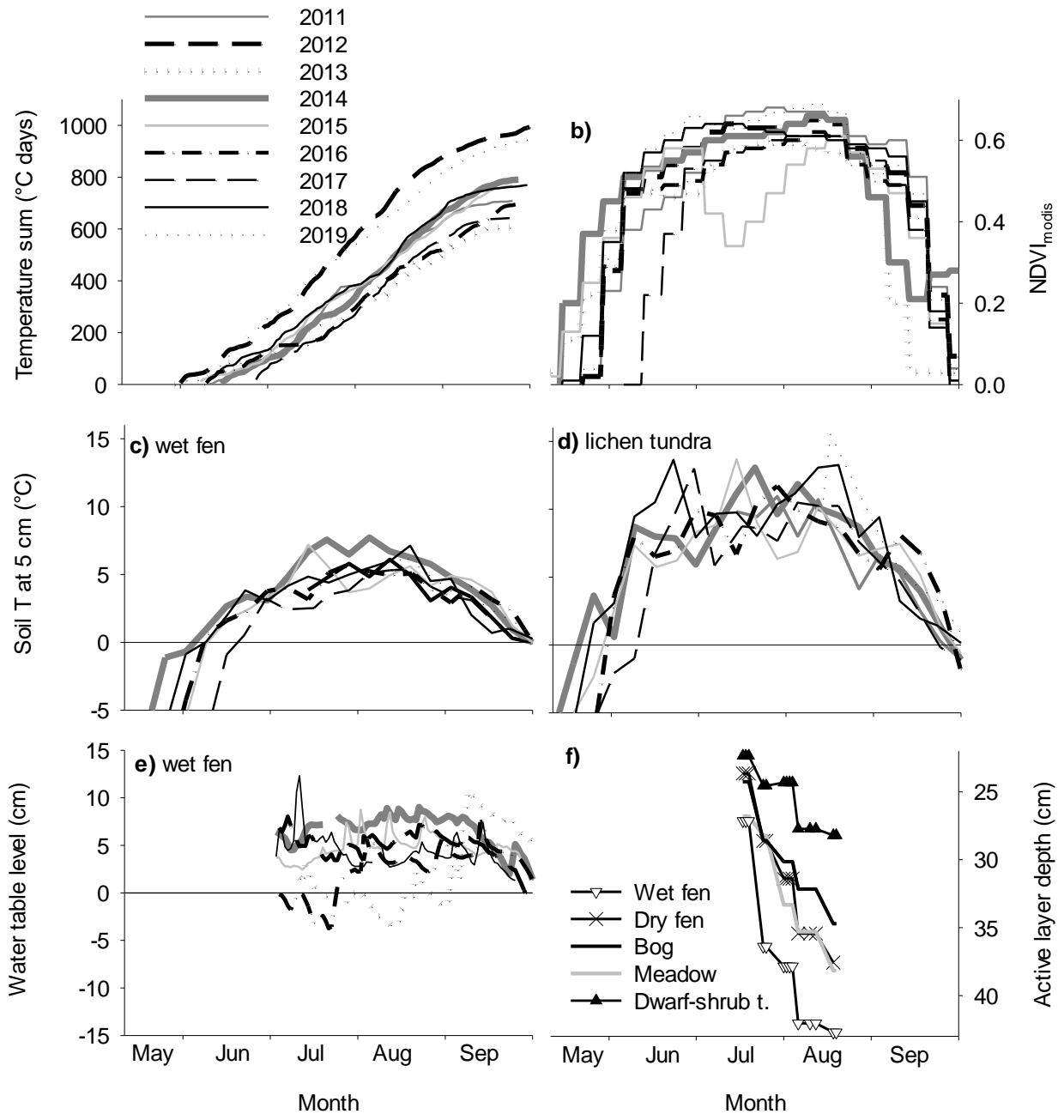
304 In 2014, when we collected most of the flux data, temperature sum accumulation (with a 0 °C  $T_{air}$   
305 threshold) was near-average during the thaw period (the period when soil surface temperature was  
306 continuously above 0 °C), but the spring and mid-growing season were warmer than on average  
307 (Fig. 2a). The average air temperature was 15 °C during the gas flux measurements. Accordingly,  
308 the MODIS NDVI showed an early start of greening (Fig. ~~2b-d~~2b), and vegetation development had  
309 already started at the beginning of the measurement period. In ~~2010~~2011–2019, which included the

310 other CH<sub>4</sub> measurement years, the thaw period lasted for 74–124 days, creating a temperature sum  
311 range of 642–1003 °C days (Fig. 2a). Surface soils thawed between May 28 and July 9 and froze  
312 again between September 21 and October 1. Among the observation years, the years 2012 and 2019  
313 had notably longer and warmer thaw periods than the other years. The driest habitat, lichen tundra,  
314 with least snow accumulation, thawed 10–15 days earlier than the other habitats, and had a ca. 3 °C  
315 higher soil temperature than the wet fen at the depth of 5 cm (Fig. 2c-db-e). Water table depth,  
316 measured at a wet fen location, showed only subtle interannual variation (Fig. 2e). In 2014, the  
317 active layer depth, measured over the measurement period close to the collars, was deepest in the  
318 end of August, reaching 30-ca. 40 cm in the wetland and meadow habitats, and remained < 30 cm  
319 in the dry dwarf-shrub tundra (Fig. 2f). Lichen tundra had rocks underneath the loose surface layer,  
320 which made it impossible to measure the actual thaw depth.

321

322





323  
 324 **Fig. 2. Meteorology in May to September in years 2011–2019.** (a) Air temperature accumulation  
 325 with threshold values soil-surface  $T_{soil} > 0$  °C and air- $T_{air} > 0$  °C, (b) seasonal dynamics of NDVI in  
 326 the study area, 16 d aggregated MODIS data, (c) weekly means of soil temperature at depth of 5 cm  
 327 in wet fen and (d) in dry tundra/lichen tundra, (e) water-table level relative to the ground surface in  
 328 wet fen, and (f) LCT means of thaw depth in the measurement collars in 2014. Rocks in the ground  
 329 prevented detecting the thaw depth of lichen tundra. ~~of the~~

330  
 331  
 332  
 333

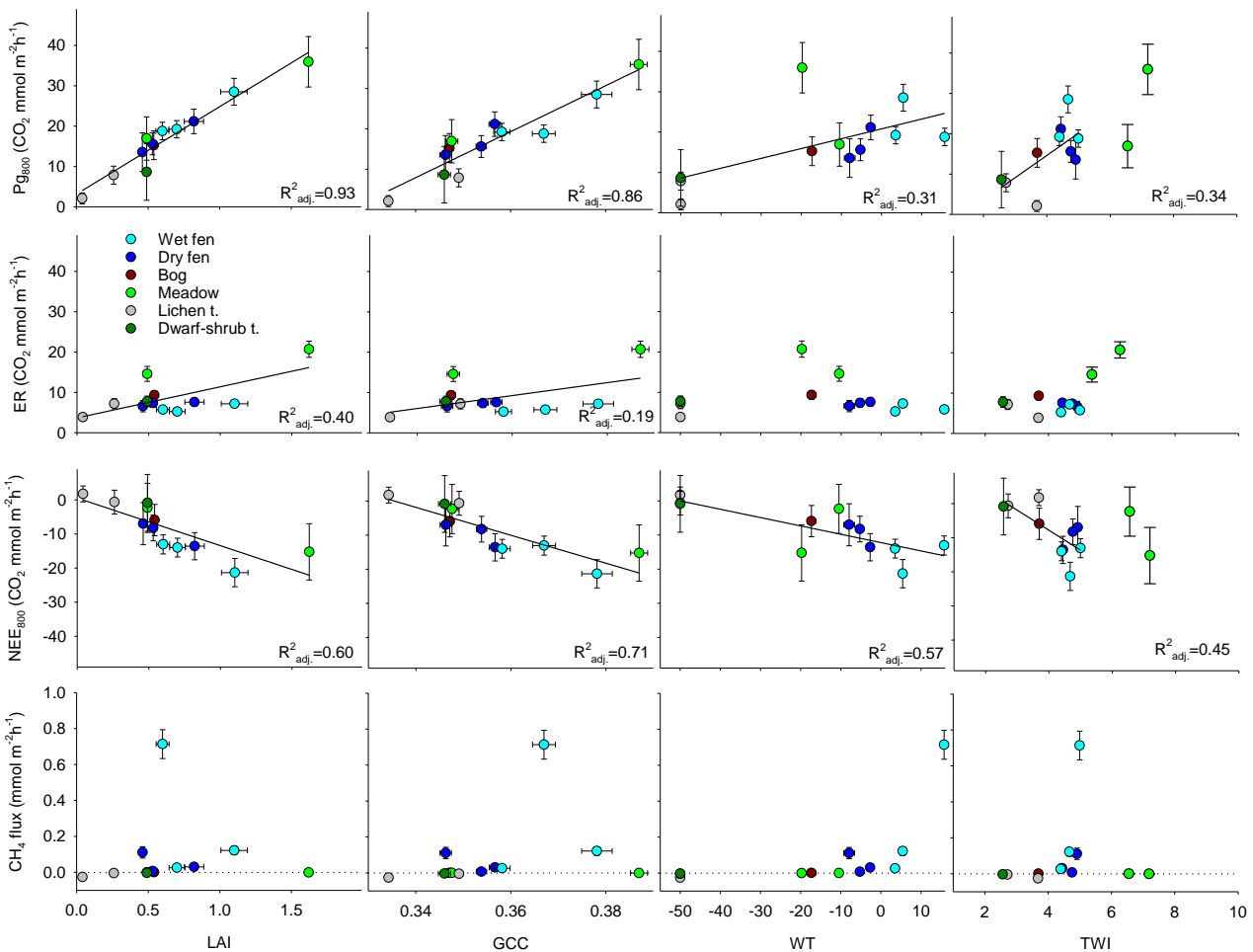
### 3.2 Exchange of CO<sub>2</sub> and CH<sub>4</sub>

334

335 Among different LCTs, the ~~light-normalized photosynthesis~~ ( $P_{g800}$ ) varied from about 5 mmol m<sup>-2</sup>  
336 h<sup>-1</sup> in the lichen tundra to about 22 and 27 mmol m<sup>-2</sup> h<sup>-1</sup> in the wet fen and meadow, respectively.  
337  $P_{g800}$  was strongly and positively ~~correlated with~~ the vascular plant LAI and the greenness index  
338 GCC (Fig. 43). There was also a positive correlation between  $P_{g800}$  and WT and TWI, possibly  
339 because the highest LAI occurred at the wet fen and meadow plots. However, the TWI values for  
340 the two meadow plots located on an elevated bank of the stream were disproportionately high in  
341 relation to the WT at the plots, probably because of insufficient locational accuracy or an artefact in  
342 the digital elevation model. Ecosystem respiration was ~~higher~~ highest in the two meadow plots, on  
343 average 18 mmol m<sup>-2</sup> h<sup>-1</sup>, ~~than in other plots~~. The relationship between ER and LAI was weaker than  
344 ~~between that of~~  $P_{g800}$  and LAI (Fig. 43). The ~~light-normalized net exchange~~,  $NEE_{800}$ , varied from  
345 about zero in the lichen tundra plots to a net CO<sub>2</sub> uptake of 16 mmol m<sup>-2</sup> h<sup>-1</sup> in the meadow and wet  
346 fen plots.  $NEE_{800}$  was more tightly linked to  $P_{g800}$  than ~~to~~ ER and was correlated with LAI, GCC,  
347 WT, and TWI (Fig. 43).

348 There was substantial consumption of the atmospheric CH<sub>4</sub> in the ~~lichen tundra~~  
349 ~~barren tundra~~ (mean  $-0.018 \pm$  standard error  $0.002$  mmol m<sup>-2</sup> h<sup>-1</sup>) and in vegetated lichen tundra  
350 (mean  $-0.006 \pm$  standard error  $0.002$  mmol m<sup>-2</sup> h<sup>-1</sup>) plots (mean  $-0.02$  mmol m<sup>-2</sup> h<sup>-1</sup>; (Figs. 5-4 and;  
351 Fig. 5). Minor consumption occurred in the meadow, dwarf-shrub tundra, and bog plots (mean  $<$ -  
352  $0.002$  mmol m<sup>-2</sup> h<sup>-1</sup>), and efflux to the atmosphere was observed in the dry fen and wet fen plots  
353 (means  $0.05$  and  $0.16$  mmol m<sup>-2</sup> h<sup>-1</sup>, respectively; Figs. 5-4 and 5). ~~The eroded bare-peat plot within~~  
354 ~~the dry fen habitat and the vehicle-track plots in wet fen had equally high emissions than the fens~~  
355 ~~The eroded bare-peat plot within the dry fen habitat and the vehicle-track plots in wet fen had large~~  
356 ~~emissions (up to  $0.2$  mmol m<sup>-2</sup> h<sup>-1</sup>), which were of the same magnitude as in the undisturbed dry~~  
357 ~~and wet fen habitats~~. Variation among the plot means ~~of CH<sub>4</sub> flux~~ (Fig. 4-3 for year 2014 data, Fig.  
358 ~~5 for all years~~) was ~~positively correlated with~~ related to WT, and ~~Large CH<sub>4</sub> emissions occurred~~

359 when TWI was  $> 4$  CH<sub>4</sub> emissions occurred when TWI  $> 4$ . Note that, except for the two meadow  
 360 plots, which that showed net consumption of CH<sub>4</sub> but and had an unrealistically high TWI relative  
 361 to their WT (see above and Figs. 43 and 65). Variation in CH<sub>4</sub> fluxes was not incoherently related  
 362 to variation in LAI or GCC, because the high emission cases in plots with little vegetation,  
 363 including the wettest wet fen plot, vehicle-track, and bare-peat plots (Fig. 5).

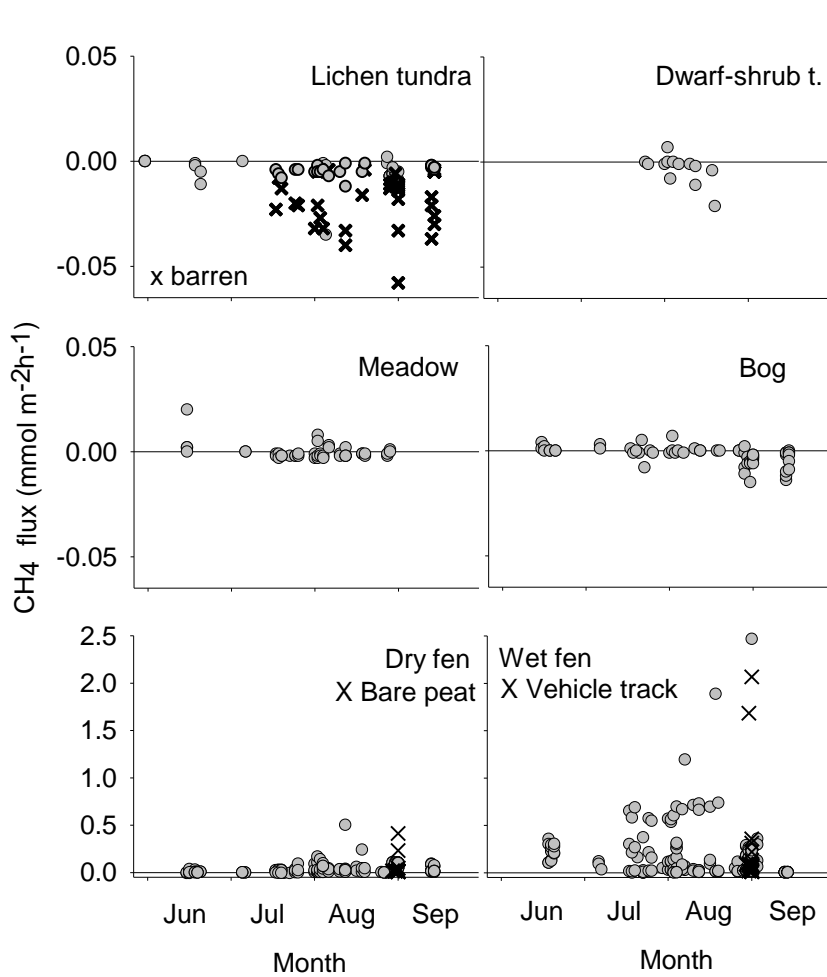


366  
 367  
 368 **Fig. 43.** Variation in estimates of Pg<sub>800</sub>, ER, NEE<sub>800</sub> (Eq. 1) and collar means of CH<sub>4</sub> fluxes in  
 369 relation to variation in collar means of LAI, GCC, WT and TWI ~~in~~ July 6–August 16, 2014. Error  
 370 bars denote the standard error of estimate. Fitted regression lines and adjusted coefficients of  
 371 determination (R<sup>2</sup><sub>adj.</sub>) are included for significant linear relationships. The two meadow plots were  
 372 not included in the TWI regressions.

373

374

375

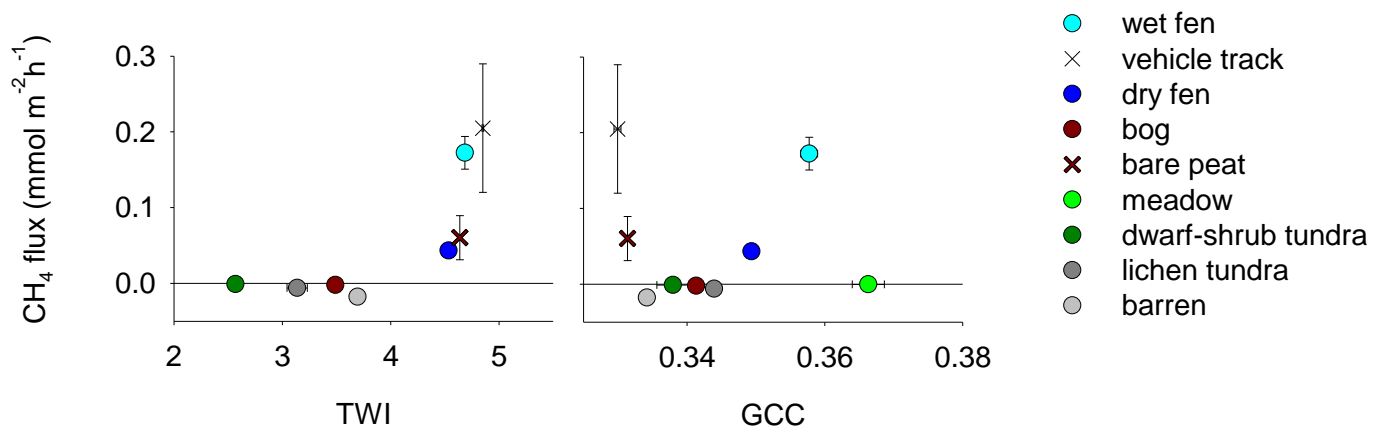


376

377 **Fig. 54.** Instantaneous (left panels) and monthly mean (right panels, with  $\pm$ SD error bars) CH<sub>4</sub>  
378 fluxes in each LTC. The data are a composite of all study years. Barren surfaces are indicated  
379 among the lichen tundra data. The eroded bare-peat and vehicle-track plots are plotted as part of the  
380 dry fen and wet fen data (x), respectively, but these data are not included in the monthly means.  
381 Note that the panel groups have different y-axis scales.

382

383

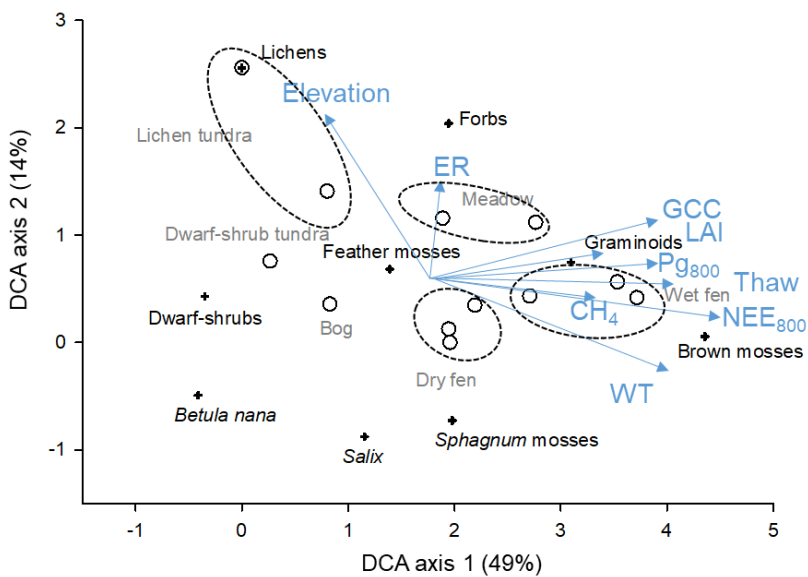


384

385 **Fig. 65.** Instantaneous CH<sub>4</sub> fluxes in the LCTs in relation to a) plot specific TWI and b) GCC and  
 386 e) LCT mean ( $\pm$ SDSE) CH<sub>4</sub> fluxes in relation to LCT mean ( $\pm$ SDSE) TWI (excluding the meadow  
 387 plots) with erroneous TWI) and d) GCC. LCT mean CH<sub>4</sub> fluxes ( $\pm$ SD). Data from years  
 388 2014, 2012–2019, 2016, and 2019.

389

390 The DCA ordination summarizes the associations with plant communities, WT, and  
 391 CO<sub>2</sub> and CH<sub>4</sub> exchange. The DCA ordination of species with post-hoc fit of environmental  
 392 variables showed that species distributed along a moisture gradient. Axis 1 explained 49 % of the  
 393 variation in the species data and distinguished the wet and dry plant communities the LCTs from  
 394 wet fen to lichen tundra (Fig. 6). Graminoids and brown mosses occurred in the wet end of the  
 395 gradient, while dwarf-shrubs, *Betula nana*, and lichens occurred in the dry end of it. The barren plot  
 396 differed most from the other plots with its negligible vegetation. Axis 2 explained additional 14 %  
 397 of the variation in the species data (Fig. 6). The supplementary variables WT, vascular plant LAI,  
 398 thaw depth, GCC, Pg<sub>800</sub>, NEE<sub>800</sub>, and CH<sub>4</sub> fluxes correlated positively with Axis 1 having post-hoc  
 399 correlations (r) of 0.6–0.9, as derived from the DCA-weighted correlation matrix. In turn, plot's  
 400 elevation and ER had positive correlations with Axis 2 (r = 0.8 and 0.4, respectively).



401

402 **Fig. 6.** DCA ordination diagram based on species (species groups) data from the measurement  
 403 collars in 2014. The explained variation in the species data is indicated for the axes 1 and 2. In the  
 404 plot, the scores of species groups (cross), sample plots (open symbols), and post-hoc fits of  
 405 supplementary variables (arrows, blue type) mean CH<sub>4</sub>, Pg<sub>800</sub>, ER, NEE<sub>800</sub>, thaw depth (Thaw),  
 406 water table relative to the ground surface (WT), green chromatic coordinate (GCC), vascular plant  
 407 LAI, and elevation above sea level (Elevation). Land-cover types of the sample plots are indicated  
 408 (grey type) and plots assigned to same LCTs are circled.

409

410

411 To compare the chamber-based flux data with those derived from the EC  
 412 measurements, the EC data were classified based on wind direction, which reflects the varying  
 413 domination of different LCTs within the EC source area. In both the southern and south-western  
 414 wind sectors (125–185° and 185–239°), ~~wet fen and graminoid tundra together contributed ca. 40%~~  
 415 ~~of the footprint weighted LCT areas (Fig. 7a). In these directions,~~ vegetation mainly consisted of  
 416 graminoids, as ~~the LCTs~~ dry fen, wet fen, graminoid tundra, and meadow ~~contributed comprised~~ 80  
 417 % ~~in of the~~ total ~~footprint-weighted area~~ (Fig. 7a). The northern sector (310–360°) was  
 418 characterized by ~~the abundance of~~ lichen tundra and bare ground that accounted for 68% of the  
 419 footprint-weighted LCT areas, while all the other LCTs covered less than 18% in total. The other  
 420 wind direction sectors had more even LCT distributions. The differences between the sectors were

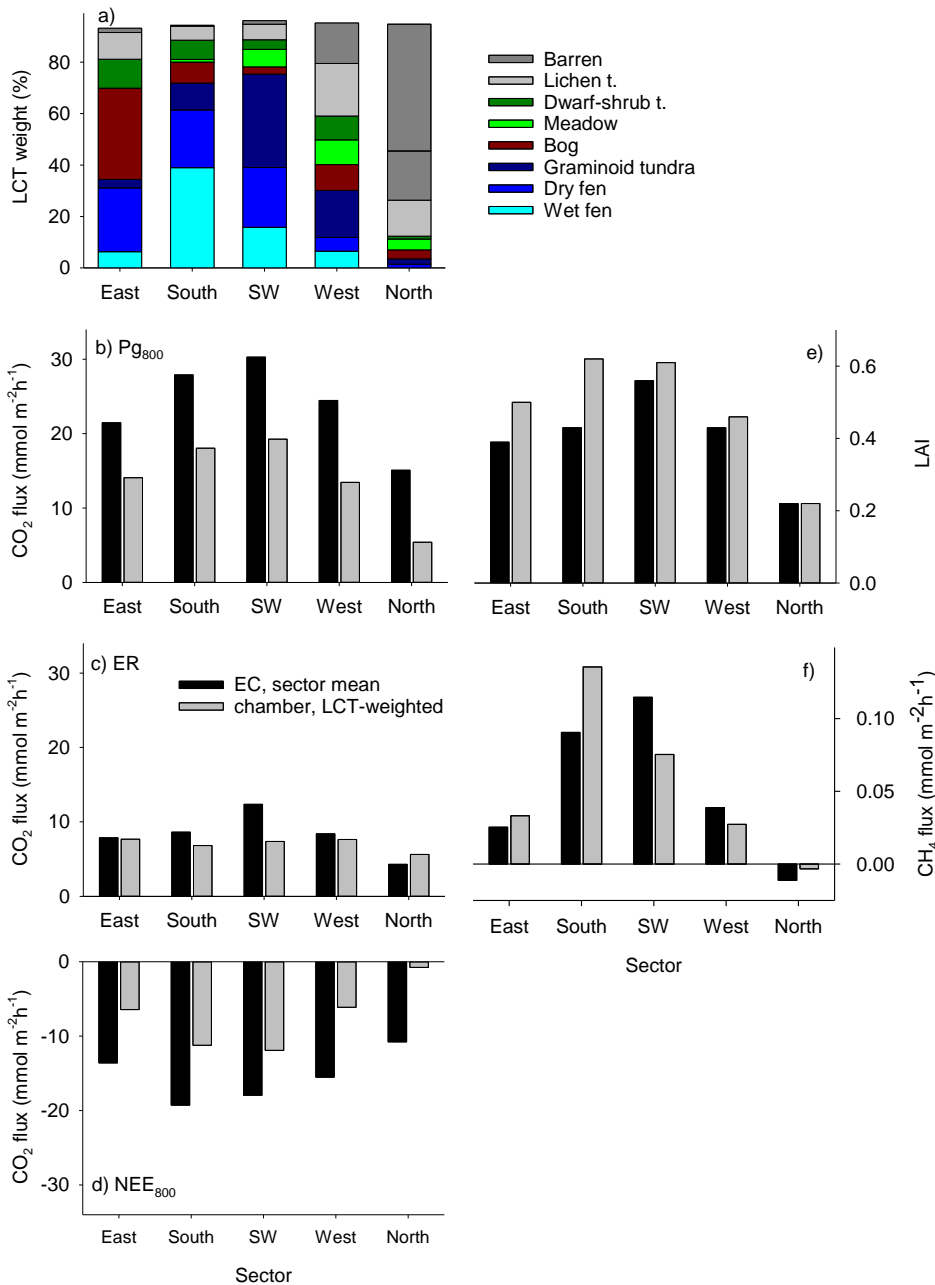
421 similar in the EC-based and spatially weighted chamber-based averages of CO<sub>2</sub> exchange (Fig. 7b–  
422 d). Both P<sub>g800</sub> and NEE<sub>800</sub> were largest in the southern and south–western sectors and clearly  
423 smallest in the barren–lichen tundra-dominated sector in the north. The chamber-based estimates of  
424 CO<sub>2</sub> exchange were, however, lower: on average P<sub>g800</sub> was 57%, ER was 93%, and NEE<sub>800</sub> was 44  
425 % of the EC-based estimate among the wind direction sectors.

426 The southern and south-western wind sectors with abundant dry and wet fens and  
427 graminoid tundra had clearly the largest CH<sub>4</sub> fluxes (Fig. 7f). The estimate based on chamber  
428 measurements was 30% and 50% larger than the EC-based estimate for the east sector (dominated  
429 by dry fen and bog) and south sector (dominated by dry and wet fen), respectively. In contrast, the  
430 chamber-based estimate was smaller than 56–67% of the EC-based estimate for the other sectors,  
431 which were, dominated by graminoid tundra, and lichen tundra, and barren ground. Both the EC-  
432 and chamber-based estimates showed consumption of atmospheric CH<sub>4</sub> for the northernmost  
433 sector, of which barren ground and lichen tundra covered 50 % and 20 %, respectively. The EC-  
434 based estimate was three times the chamber-based estimate.

435 Within the extended study area of 35.8 km<sup>2</sup>, the LCT-weighted mean NEE<sub>800</sub>,  
436 corresponding to the LCT-specific chamber-based fluxes was -4.6 mmol m<sup>-2</sup> h<sup>-1</sup> (uptake relative to  
437 the atmosphere). The corresponding mean P<sub>g800</sub> was 42–11 mmol m<sup>-2</sup> h<sup>-1</sup>, and CH<sub>4</sub> flux 0.05 mmol  
438 m<sup>-2</sup> h<sup>-1</sup> (Table 3). Relative to their spatial cover (28% in total), wet and dry fens were  
439 disproportionately important for the landscape-level net exchange of CO<sub>2</sub>, photosynthesis P<sub>g800</sub>,  
440 NEE<sub>800</sub>, and CH<sub>4</sub> emissions, because the fens, contributed ing 7447 % of total P<sub>g800</sub>, 4774 % of  
441 NEE<sub>800</sub>, and 9997 % of total CH<sub>4</sub> emission (105 % of the balance)-the net landscape totals- (Table  
442 3). Consumption of CH<sub>4</sub> by barren and lichen tundra (including barrens), dwarf-shrub tundra, and  
443 meadow tundra soils was contributed -9 % of the CH<sub>4</sub> balance, and the barren dominated the sink.  
444 10% of the CH<sub>4</sub> emission. Particularly, the barrens contributed ed to the consumption  
445 of CH<sub>4</sub> due it to their large area and high consumption rate. Note, however, that the EC-based



446 estimates for the wind direction sectors suggested about two times as high  $NEE_{800}$  and ca. 30%  
 447 smaller  $CH_4$  emissions for the wet fens, and 30% larger consumption for the barrens and lichen  
 448 tundra.  
 449  
 450



451  
 452 **Fig. 7.** Footprint-weighted mean contribution of each LCT to the EC measurements divided into  
 453 wind direction sectors (a), and comparison of EC and chamber-based sector means of (b-d)  $CO_2$   
 454 exchange ( $Pg_{800}$ , ER, and  $NEE_{800}$  (b-d)), (e) vascular plant LAI (e), and (f)  $CH_4$  fluxes (f). The  
 455 chamber-based data are weighted by the LCT proportions shown in panel a. All data were measured

456 in 2014. Map of LAI (Tuovinen et al., 2019) and the LAI measured in the collars were used to  
 457 estimate the EC- and chamber-related sector means, respectively.

458

459 Table 3. Land-cover type distribution in the mapped 35.8 km<sup>2</sup> area, spatially weighted and LCT-  
 460 specific means of Pg<sub>800</sub>, ER, NEE<sub>800</sub>, and CH<sub>4</sub>, and proportions of LCTs in landscape totals of Pg<sub>800</sub>,  
 461 NEE<sub>800</sub> (% of sinks), and CH<sub>4</sub> fluxes (% of emissions). Standard error of mean (SE) is shown given  
 462 for the LCT-specific estimates. Data period: July 15 – August 16, 2014.

LCT	Area (%)	Pg <sub>800</sub> (mmol m <sup>-2</sup> h <sup>-1</sup> )		ER (mmol m <sup>-2</sup> h <sup>-1</sup> )		NEE <sub>800</sub> (mmol m <sup>-2</sup> h <sup>-1</sup> )		CH <sub>4</sub> flux (mmol m <sup>-2</sup> h <sup>-1</sup> )		Pg <sub>800</sub> (%)	NEE <sub>800</sub> (%)	CH <sub>4</sub> flux (%)
		mean	SE	mean	SE	mean	SE	mean	SE			
Mean		11.2		6.6		-4.6		0.05				
Wet fen	16.4	21.9	2.5	6.4	0.7	-15.5	3.2	0.29	0.05	32.1	55.1	94.5
Dry fen	11.6	14.6	3.5	7.0	1.1	-7.6	4.6	0.05	0.01	15.1	19.1	11.2
Gram. t.	3.4	21.9	2.5	6.4	0.7	-15.5	3.2	0.05	0.01	6.7	11.4	3.3
Bog	9.1	15.3	3.6	9.3	1.0	-5.9	4.6	0.0001	0.0005	12.4	11.7	0.0
Meadow	0.4	26.4	5.8	17.7	1.9	-8.8	7.7	-0.001	0.0004	0.9	0.8	0.0
Dwarf-s. t.	27.4	8.6	7.0	7.8	1.3	-0.8	8.3	-0.003	0.0015	21.1	5.0	-1.8
Lichen t.	11.1	5.0	2.2	5.5	1.3	0.5	3.5	-0.005	0.001	4.9	-1.3	-1.1
Barren	15.3	5.0	1.4	5.5	1.0	0.5	2.3	-0.020	0.003	6.8	-1.8	-6.1
Water	5.3	NA		NA		NA		NA				

463 mean, <sup>2</sup>Graminoid tundra fluxes estimated using values for wet fen (CO<sub>2</sub>) and dry fen (CH<sub>4</sub>)

464

465

#### 466 4 Discussion

467 The studied tundra site in Tiksi in northeastern Siberia has heterogeneous land cover, which is  
 468 reflected as equally heterogeneous CO<sub>2</sub> and CH<sub>4</sub> exchange. ~~On the one hand, w~~We found, ~~however,~~  
 469 that the ~~tundra wetlands~~LAI of vascular plants was a robust predictor of Pg<sub>800</sub> and NEE<sub>800</sub> across  
 470 ~~the LCTs. Due to the distribution of species and LAI, the have a disproportional role: dry and wet~~  
 471 ~~fens and meadow~~ tundra wetlands had a ~~disproportionate~~ role ~~in~~of the landscape-level ~~the highest~~  
 472 CO<sub>2</sub> uptake capacity. ~~The fens also dominated the landscape's CH<sub>4</sub> emissions. On the other hand,~~  
 473 ~~our results highlight the differences in CH<sub>4</sub> consumption rates among the dry tundra. In total~~  
 474 ~~consumption of the atmospheric CH<sub>4</sub> by dry tundra was -9 % of the total CH<sub>4</sub> balance within this~~  
 475 ~~landscape, but the consumption rate at barren surface was much higher that in other dry tundra~~  
 476 ~~habitats and this finding is in agreement with other studies (Table 4). In Tiksi, the barren was~~

477 characterized by sand and rocks (Fig. A1). The consumption of CH<sub>4</sub> was smaller if the sand and  
478 stones were partly covered with vegetation and, in lichen tundra, with a thin organic layer (Figs. 5  
479 and A1).  
480 ~~and particularly the wet fen showed high CH<sub>4</sub> emissions. On the other hand, our results highlight~~  
481 ~~the high was with consumption of atmospheric CH<sub>4</sub> by lichen tundra (barrens and small vegetated~~  
482 ~~patches). This CH<sub>4</sub> consumption is high compared to other non-wetland tundra habitats In Tiksi,~~  
483 ~~the barren was characterized by sand and rocks (Appendix fFig. A1). The consumption of CH<sub>4</sub> was~~  
484 ~~smaller if the sand and stones were partly covered by with some vegetation and, in lichen tundra,~~  
485 ~~with a thin organic layer in lichen tundra (Figs. 5 and Appendix Fig.A1). – and, on the landscape~~  
486 ~~scale, could offset 9 of the CH<sub>4</sub> emissions. These data augment the knowledge on the functional~~  
487 ~~diversity, namely the distribution of different land cover types, and their emission factors, across~~  
488 ~~the vast arctic tundra and will lend support to bottom-up and top-down extrapolations across the~~  
489 ~~Arctic.~~

490 ~~Within this tundra landscape, the graminoid-dominated wetlands with organic-rich soils~~  
491 ~~constitute an important part of the ecosystem-atmosphere exchange of CO<sub>2</sub> and CH<sub>4</sub>. Within an area~~  
492 ~~of 35.8 km<sup>2</sup> mapped around our study site (Mikola et al. 2018), wet and dry fens and the fen-like~~  
493 ~~graminoid tundra covered 31% of the area but contributed as much as 73% to the potential light-~~  
494 ~~saturated CO<sub>2</sub> sink during the peak growing season. These wetlands are also the sites having high~~  
495 ~~soil organic matter content and C pools (Mikola et al. 2018) and CH<sub>4</sub> emissions to the atmosphere~~  
496 ~~(see also Tuovinen et al. 2019).~~

497 The land-cover categorical approach serves to distinguish the basic features of spatial  
498 variation in CO<sub>2</sub> and CH<sub>4</sub> fluxes. The extreme ends of the moisture and vegetation gradients from  
499 barren to wet fen are clearly distinguishable, also in terms of CO<sub>2</sub> and CH<sub>4</sub> exchange (Fig. 6).  
500 Overall, moisture gradient, vegetation types and ecosystem functions are connected and manifested  
501 for example, as distribution of barren ground where wind sweeps snow away and highed thaw depth,

502 [on the other hand, in depressions with snow accumulation \(Fig. 6, Callaghan et al. 2011\).](#)  
503 [Nevertheless, the spatial extrapolation of fluxes is clearly sensitive to a small number of chamber](#)  
504 [measurement points as there is large within-LCT variation, as observed in the wet fen and meadow](#)  
505 [data, which originates from plot-to-plot variation in LAI. The LCTs share common features and](#)  
506 [form a continuum as shown in DCA ordination \(Fig. 6\). Mikola et al. \(2018\) used a larger data set](#)  
507 [and found also that the neighboring LCTs overlapped in terms of soil properties and vegetation.](#)  
508 [Our conclusions made from the chamber data are, however, corroborated by the temporally](#)  
509 [matching section of EC data, categorized by wind direction to reflect the main LCT patterns around](#)  
510 [the EC mast, which show similarity to the chamber data \(Fig. 7\). Furthermore, the statistical](#)  
511 [analysis of EC data by Tuovinen et al. \(2019\) showed that it is possible to find significant](#)  
512 [differences between different LCT categories representing high and low CH<sub>4</sub> emitters and CH<sub>4</sub>](#)  
513 [sinks. For spatial modeling of ecosystem functions, however, maps of key variables, such as LAI](#)  
514 [and WT, that drive CO<sub>2</sub> and CH<sub>4</sub> exchange would be preferable to categorical LCT classification](#)  
515 [\(Räsänen et al. 2021\).](#)

516           The spatial pattern of the growing season ~~light-saturated photosynthesis~~  $P_{g800}$  and ~~net~~  
517 ~~CO<sub>2</sub> exchange~~  $NEE_{800}$  was strongly related to the corresponding pattern of the LAI of vascular  
518 plants (Figs. 3, and 4). Hence, the abundance of graminoid (Cyperaceae and Poaceae) vegetation  
519 predicted a large  $NEE_{800}$ , which varied from near zero in lichen tundra up to 25 mmol m<sup>-2</sup> h<sup>-1</sup> in wet  
520 fen. Ecosystem respiration had a smaller role than  $P_g$  in determining NEE, but we note that our data  
521 cover only a section of the growing season with warmer temperatures and half to full-grown  
522 vegetation. The importance of ER is likely to be different when considering the full annual balance  
523 (e.g., Hashemi et al. 2021). While our data represent only the growing season, a similar relationship  
524 has also been found between the annual NEE and LAI at a tundra site with a mixture of wet and dry  
525 tundra in northeastern Europe (Marushchak et al. 2013), in a multi-site EC study in Alaskan tundra

526 (McFadden et al. 2003), in Canadian low arctic tundra wetlands (Lafleur et al. 2012), and across  
527 tundra sites (Street et al. 2007; Shaver et al. 2007).

528 The magnitude of  $P_{g800}$  and  $NEE_{800}$  in the fen and meadow plots of this study were  
529 similar to the maximum  $P_g$  and  $NEE$  found in tundra wetland in Seida in northeastern Europe  
530 (Marushchak et al. 2013), at low tundra wetland sites in eastern Canada (Lafleur et al. 2012), and at  
531 a wetland-dominated but more continental site (with an equal growing season length) in  
532 northeastern Siberia (van der Molen et al. 2007). The vegetation and  $P_{g800}$  of lichen tundra and  
533 dwarf-shrub tundra in our study resembled those observed within the polygon rim habitat of the  
534 polygon tundra in the Lena River delta, while those of meadow, dry fen, and wet fen resembled the  
535 wet polygon center habitats (Eckhardt et al. 2019). In our study, the variation of ecosystem  
536 respiration resulted from the variation in vascular plant LAI, soil organic content, and water  
537 saturation: the highest ER occurred in mineral soil meadow with high LAI suggesting substantial  
538 autotrophic respiration and likely deep rooting and large root biomass contributing to the ecosystem  
539 respiration (Fig. 4). ~~In wetlands, respiration may be attenuated by the soil water saturation.~~

540 Our chamber-based estimate of the average  $CH_4$  flux within the 35.8 km<sup>2</sup> upscaling area  
541 was 0.05 mmol m<sup>-2</sup> h<sup>-1</sup>, which is close to 0.04 mmol m<sup>-2</sup> h<sup>-1</sup> obtained by Tuovinen et al. (2019), who  
542 combined EC data with footprint modeling to statistically determine LCT group-specific  $CH_4$   
543 fluxes. Within this upscaling area, ~~we estimate that~~ 28% of the area emitted  $CH_4$ , while the other  
544 habitats either consumed atmospheric  $CH_4$  (~~barrens and~~ lichen tundra, ~~dwarf-shrub tundra,~~  
545 ~~meadow) including barrens, coverage 26%)~~ or were close to neutral relative to the atmosphere  
546 (Figs. 4, 5, Table 3). ~~The wettest spots were the sites having the highest  $CH_4$  emissions (Fig. 4).~~  
547 ~~The relationship between vascular plant LAI and  $CH_4$  flux was confused We observed no clear~~  
548 ~~relationship between vegetation and  $CH_4$  flux in plot level, which by the occurrence of large  $CH_4$~~   
549 ~~fluxes in plots with little or no vegetation. Those cases occurred at were the wettest fen plot, and~~  
550 ~~bare-peat and vehicle track plots (Figs. 4–6). could partly be due to the small size of data. At a LCT~~

551 ~~level, high~~ High LAI, high WT and ~~and~~ high CH<sub>4</sub> emissions systematically co-occurred ~~if WT was~~  
552 high enough in wet fen (Fig. 36). ~~The sites showing the highest emissions had a high soil organic~~  
553 ~~matter content, an indication of slow decomposition in anoxic conditions, and we also found that~~  
554 ~~The eroded bare-peat surface of dry fen and the disturbed vehicle tracks had high CH<sub>4</sub> emissions,~~  
555 where. ~~In the case of eroding surfaces, gas efflux may be enhanced by transport pathways emerging~~  
556 ~~from changes in soil structure. Wet depressions, like the vehicle tracks in this study, have in turn~~  
557 ~~been found to have high CH<sub>4</sub> emissions relative to their surroundings in permafrost, erosion or~~  
558 disturbance may have created CH<sub>4</sub> flux hotspots due co-occurrence of permafrost scars, water  
559 saturation, and recently thawed organic matter ~~which results from the abundance of graminoids~~  
560 ~~producing easily degradable litter compared to dwarf shrubs, and the potentially increasing~~  
561 ~~nutrients from seasonal permafrost degradation~~ (e.g., Bubier et al. 1995, McCalley et al. 2014,  
562 Wickland et al. 2020). ~~These are small--scale landscape features, while in a larger scale, All in all,~~  
563 our data encourage applying indicators-indices of wetness ~~together with and vegetation~~ vegetation  
564 parameters as a means of CH<sub>4</sub> flux upscaling in tundra environment. ~~While the topographic wetness~~  
565 ~~index in general was a reasonable surrogate for WT, distinguishing the dry and wet soils, erroneous~~  
566 ~~TWI values were estimated for the streamside meadow, possibly due to insufficient locational~~  
567 ~~accuracy, because the plots were located right next to the stream, but on an elevated bank.~~

568 The recognition of CH<sub>4</sub> consuming tundra habitats is important for accurately estimating  
569 the net CH<sub>4</sub> balance of tundra. The substantial uptake of atmospheric CH<sub>4</sub> by lichen tundra (here a  
570 mixture of bare ground and sparse vegetation) in Tiksi was inferred by Tuovinen et al. (2019) based  
571 on a source allocation analysis of EC data: the average flux of the consuming area was estimated at  
572  $-0.03 \text{ mmol m}^{-2} \text{ h}^{-1}$ , which ~~corresponds~~ corresponded to  $-21.6\%$  of the total upscaled CH<sub>4</sub> flux. In  
573 this study, the average growing-seasonal CH<sub>4</sub> uptake was  $-0.02 \text{ mmol m}^{-2} \text{ h}^{-1}$  in the lichen tundra  
574 plots ~~barren tundra and~~ ~~and~~ an order of magnitude lower in vegetated lichen tundra, graminoid  
575 tundra, dwarf-shrub tundra, and bog. Our upscaling exercise ~~resulted in~~ suggested a CH<sub>4</sub> sink that

576 ~~counterbalanced about~~ corresponded -10-9 % of the CH<sub>4</sub> emission balance. It is n measurements a  
577 (Fig. 7; Tuovinen et al., 2019) This difference may originate from the LCT-weighting and the small  
578 sample of the chamber-based estimate.

579 ~~;~~ which likely is an underestimate due to an overestimation of the emissions from the  
580 ~~wet fens.~~ High consumption of atmospheric CH<sub>4</sub> in barrens is associated with the high affinity  
581 methanotrophs ((Emmerton et al. 2014, Jørgensen et al. 2014; Lau et al. 2015; D'Imperio et al.  
582 2017, St Pierre et al. 2019). In our summary review of CH<sub>4</sub> fluxes in table for mineral-rich dry tundra  
583 (Table 4), the consumption values of this study and Tuovinen et al. (2019) are the highest, but  
584 similar rates consumption of same magnitude have been observed in other dry tundra sites with little  
585 or no vegetation. For instance, on Disko Island, Greenland, which consists of similar land cover  
586 types to Tiksi, uptake of CH<sub>4</sub> by bare ground was -0.005–0.01 mmol m<sup>-2</sup> h<sup>-1</sup> during the growing  
587 season, while a mean flux of -0.003–0.004 mmol m<sup>-2</sup> h<sup>-1</sup> was observed in dry tundra heath  
588 (D'Imperio et al. 2017). These consumption rates associated with tundra barrens and high-affinity  
589 methanotrophs can be even higher than those relative to consumption rates measured on north-  
590 boreal forest soils (for instance, -0.01 mmol m<sup>-2</sup> h<sup>-1</sup>, Lohila et al. 2016).

591  
592 Table 4. Summary of reported consumption rates of atmospheric CH<sub>4</sub> in dry mineral soil tundra.

Location	Habitat type	Mean ( $\mu\text{mol m}^{-2}\text{h}^{-1}$ )	Min	Max	Reference
Narsarsuaq, Greenland	low elevation heath vegetation	-1.2	-4.0	-0.2	St Pierre et al. 2019
Narsarsuaq, Greenland	high elevation heath vegetation	-2.6	-11.9	3.6	St Pierre et al. 2019
Disko Island-, Greenland	low elevation heath vegetation	-3.8	-12.1	-1.1	St Pierre et al. 2019
Disko Island-, Greenland	high elevation heath vegetation	-3.5	-12.1	-1.3	St Pierre et al. 2019
Tierra del Fuego, Argentina	alpine tundra	0.5	-16.6	10.3	Sá et al. 2019
Disko Island-, Greenland	dry tundra heath <sup>1</sup>	-4.0	-4.4	-2.5	D'Imperio et al. 2017
Disko Island-, Greenland	bare ground <sup>1</sup>	-9.0	-15.0	-3.8	D'Imperio et al. 2017
Disko Island-, Greenland	Betula nana and Salix sp. heath	-4.0			Christiansen et al. 2014
Axel Heiberg Island, CA	vegetated ice-wedge polygon		-2.7	-0.3	Lau et al. 2015
Lake Hazen, Ellesmere I., CA	polar desert <sup>2</sup>	-3.6	-7.0	0.0	Emmerton et al. 2014
Zackenber Valley, Greenland	moist tundra	-3.1	-7.0	-2.0	Jørgensen et al. 2014
Zackenber Valley, Greenland	dry tundra & barren ground	-7.0	-16.0	-4.0	Jørgensen et al. 2015



Zackenbergl Valley, Greenland	tundra heath	-1.3	-6.0	0.0	Christensen et al. 2000
Okse Bay, Ellesmere I., CA	polar desert <sup>3</sup>	-0.5			Brummel et al. 2014
Petterson R., Ellesmere I., CA	polar desert <sup>3</sup>	-0.04			Brummel et al. 2014
Dome, Ellesmere I., CA	polar desert <sup>3</sup>	-0.5			Brummel et al. 2014
BAWLD-CH <sub>4</sub> Synthesis	dry tundra		-2.9	5.2	Kuhn et al. 2021
BAWLD-CH <sub>4</sub> Synthesis	boreal forest		-2.6	-0.5	Kuhn et al. 2021
<a href="#">Tiksi, RU</a>	<a href="#">Barren &amp; lichen tundra</a>	<a href="#">-29</a>			<a href="#">Tuovinen et al. 2019</a>
Tiksi, RU	lichen tundra mean	-11.3	-57.9	-0.4	This study
Tiksi, RU	barren	-18.1	-57.9	-3.0	This study
Tiksi, RU	vegetated	-6.0	-34.7	-0.4	This study
Tiksi, RU	meadow	-1.0	-21.1	24.5	This study
Tiksi, RU	dwarf-shrub tundra	-0.2	-2.9	20.3	This study
Tiksi, RU	bog	-2.1	-14.8	6.6	This study

593 1) mean estimated from a figure, 2) min and max estimated from a figure, 3) one-three day  
594 measurement, 4) <sup>4)</sup> estimated from EC measurements with a statistical model.

595  
596

## 597 5 Conclusions

598 Our results provide new observations of carbon exchange for the prostrate dwarf shrub tundra sub-  
599 zone, which covers ~~a substantial~~ <sup>an</sup> area of 2.3 million km<sup>2</sup> of the Arctic (Walker 2000). [These data](#)  
600 [augment the knowledge on the functional diversity, namely the distribution of different land-cover](#)  
601 [types and their emission factors, across the vast arctic tundra and will lend support to bottom-up and](#)  
602 [top-down extrapolations across the Arctic.](#) Graminoid vegetation favored the wet and moist  
603 habitats, such as wet fens ~~and the streamside meadow~~, which were characterized by large CO<sub>2</sub>  
604 uptake and CH<sub>4</sub> emissions. [In addition, our data supports the observation of notable consumption of](#)  
605 [atmospheric CH<sub>4</sub> in barren tundra that has substantial coverage across the Arctic.](#) The heterogeneity  
606 of landscape and the related large spatial variability of CO<sub>2</sub> and CH<sub>4</sub> fluxes observed in this study  
607 encourage to monitor the Arctic sites for changes in habitat type distribution. Such changes can  
608 include the forming of meadows [and wet fens](#) -and appearance of new vegetation communities, such  
609 as erect shrubs, that benefit of warming-induced changes in thaw depth and soil wetness. The  
610 spatial extrapolation based on a small number of measurement points involves inherent uncertainty

611 but still allowed us to identify key relationships between CO<sub>2</sub> and CH<sub>4</sub> fluxes and vegetation and  
612 moisture features, which can be utilized in more robust upscaling experiments that make use of EC  
613 measurements.

614

615 *Data availability.* The flux data used in this study can be accessed via the Zenodo data repository:

616 Juutinen, Sari. (2022). Dataset for a manuscript entitled Variation in CO<sub>2</sub> and CH<sub>4</sub> Fluxes Among

617 Land Cover Types in Heterogeneous Arctic Tundra in Northeastern Siberia [Data set]. Zenodo.

618 <https://doi.org/10.5281/zenodo.5825705>

619

620

621

622 *Author contributions*

623 TL, MA, and SJ designed the study. TL, MA, and AM took care of the overall site governance and

624 maintenance. VI, ML, TL, JM, JN, EV, TL, TV, and MA conceived the field measurements of CO<sub>2</sub>

625 and CH<sub>4</sub>, vegetation, and environmental variables. In addition, ML calculated green chromatic

626 coordinates, and MA and J-PT postprocessed the EC data and J-PT modeled the footprint and

627 estimated footprint LCT fractions. AR and TV processed and modelled the landcover data and

628 estimated TWI and NDVI for the plots and area. SJ compiled the chamber flux data and conducted

629 the data analyses and spatial extrapolations and wrote the manuscript with contributions from all co-

630 authors.

631

632 *Competing interests*

633 The authors declare that they have no conflict of interest.

634

635 *Acknowledgements*

636 We thank G. Chumachenko, O. Dmitrieva, and E. Volkov at the Tiksi Observatory and the  
637 Yakutian Hydrometeorological Service for their kind assistance in carrying out and organizing the  
638 field campaigns and Lauri Rosenius for assistance in the field work. This study was financially  
639 supported by the Academy of Finland, projects “Greenhouse gas, aerosol and albedo variations in  
640 the changing Arctic” (project no. 269095), “Carbon balance under changing processes of Arctic and  
641 subarctic cryosphere” (project no. 285630), “Constraining uncertainties in the permafrost-climate  
642 feedback” (project no. 291736) and “Carbon dynamics across Arctic landscape gradients: past,  
643 present and future” (project no. 296888); the European Commission, FP7 project “Changing  
644 permafrost in the Arctic and its global effects in the 21st century (PAGE21, project no. 282700”);  
645 and the Nordic Council of Ministers, DEFROST Nordic Centre of Excellence within NordForsk.

646

## 647 **References**

- 648 AARI: Archive of Tiksi standard meteorological observations (1932–2016), Russian Federal  
649 Service for Hydrometeorology and Environmental Monitoring, St Petersburg, Russia,  
650 available at: [http://www.aari.ru/resources/d0024/archive/description\\_e.html](http://www.aari.ru/resources/d0024/archive/description_e.html), last  
651 access: 13 September 2018.
- 652 Aurela, M., Laurila, T., and Tuovinen, J-P.: The timing of snow melt controls the annual CO<sub>2</sub>  
653 balance in a subarctic fen, *Geophysical Research Letters* 31, L16119,  
654 doi:10.1029/2004GL020315, 2004.
- 655 Brummel, M.E., Farrell, R.E., Hardy, S.P., and Siciliano, S.D., Greenhouse gas production and  
656 consumption in High Arctic deserts, *Soil Biology and Biochemistry*, 68, 158–165,  
657 <https://doi.org/10.1016/j.soilbio.2013.09.034>, 2014.
- 658 Bartlett, K. B., and Harriss, R. C., Review and assessment of methane emissions from wetlands.  
659 *Chemosphere*, 26, 261–320, 1993.

660 Bubier, J.L., Moore, T.R., Bellisario, L., Comer, N.T., and Crill, P.M: Ecological controls on  
661 methane emissions from a northern peatland complex in the zone of discontinuous  
662 permafrost, Manitoba, Canada. *Global Biogeochemical Cycles* 9. 455–470, 1995.

663 Callaghan, T.V., Johansson, M., Brown, R.D. et al. Multiple Effects of Changes in Arctic Snow  
664 Cover, 2011, *AMBIO* 40, 32–45 (2011). <https://doi.org/10.1007/s13280-011-0213-x>

665 Chen, L., Aalto, J., and Luoto, M.: Significant shallow–depth soil warming over Russia during the  
666 past 40 years. *Global and Planetary Change*, 197, 103394,  
667 [doi.org/10.1016/j.gloplacha.2020.103394](https://doi.org/10.1016/j.gloplacha.2020.103394), 2021.

668 Christensen, T. R., Friberg, T., Sommerkorn, M., Kaplan, J., Illeris, L., Soegaard, H., Nordstroem,  
669 C., and Jonasson, S., Trace gas exchange in a high-Arctic valley: 1. Variations in CO<sub>2</sub>  
670 and CH<sub>4</sub> Flux between tundra vegetation types, *Global Biogeochemical Cycles*, 14,  
671 701– 713, [doi:10.1029/1999GB001134](https://doi.org/10.1029/1999GB001134), 2000.

672 Christiansen, J.R., Romero, A.J.B., Jørgensen, N.O.G., Glaring, M.A., Jørgensen, C.J., Berg, L.K.,  
673 Elberling, B. Methane fluxes and the functional groups of methanotrophs and  
674 methanogens in a young Arctic landscape on Disko Island, West Greenland,  
675 *Biogeochemistry*, 122, 15–33, 2014.

676 D’Imperio, L., Skov Nielsen, C., Westergaard-Nielsen, A., Michelsen, A., and Elberling, B.:  
677 Methane oxidation in contrasting soil types: responses to experimental warming with  
678 implication for landscapeintegrated CH<sub>4</sub> budget. *Global Change Biology* 23, 966–  
679 976, [doi: 10.1111/gcb.13400](https://doi.org/10.1111/gcb.13400), 2017.

680 Eckhardt, T., Knoblauch, C., Kutzbach, L., Holl, D., Simpson, G., Abakumov, E., and Pfeiffer, E-  
681 M.: Partitioning net ecosystem exchange of CO<sub>2</sub> on the pedon scale in the Lena River  
682 Delta, Siberia. *Biogeosciences* 16, 1543–1562, [doi:10.5194/bg-16-1543-2019](https://doi.org/10.5194/bg-16-1543-2019), 2019.

683 Emmerton, C.A., St Louis, V.L., Lehnherr, I., Humphreys, E.R., Rydz, E., Kosolofski, H.R. The net  
684 exchange of methane with high Arctic landscapes during the summer growing season.  
685 *Biogeosciences*, 11, 3095–3106, 2014.

686 Euskirchen, E.S., Bret-Harte, M.S., Shaver, G.R., Edgar, C.W., and Romanovsky, V.E.: Long-Term  
687 Release of Carbon Dioxide from Arctic Tundra Ecosystems in Alaska. *Ecosystems* 20,  
688 960–974, doi: 10.1007/s10021-016-0085-9, 2017.

689 Gorelick, N., Hancher, M., Dixon, M., Ilyushchenko, S., Thau, D., and Moore, R.: Google Earth  
690 Engine: Planetary-scale geospatial analysis for everyone. *Remote Sensing of*  
691 *Environment*, 202, 18-27, doi.org/10.1016/j.rse.2017.06.031, 2017.

692 Hashemi, J., Zona, D., Arndt, K.A., Kalhori, A., and Oechel, W.C.: Seasonality buffers carbon  
693 budget variability across heterogeneous landscapes in Alaskan Arctic Tundra.  
694 *Environ. Res. Lett.* in press <https://doi.org/10.1088/1748-9326/abe2d1>, 2021.

695 Humphreys, E.R. and Lafleur, P.M.: Does earlier snowmelt lead to greater CO<sub>2</sub> sequestration in  
696 two low Arctic tundra ecosystems? *Geophysical Research Letters* 38, L09703,  
697 doi:10.1029/2011GL047339, 2011.

698 IPCC Summary for Policymakers in *Climate Change 2013: The Physical Science Basis* (eds  
699 Stocker, T. F. et al.) 3–29, Cambridge Univ, Press, 2013.

700 Jørgensen, C.J., Lund Johansen, K.M., Westergaard-Nielsen, A., and Elberling, B.: Net regional  
701 methane sink in High Arctic soils of northeast Greenland. *Nature Geoscience* 8, doi:  
702 10.1038/NGEO2305, 2014.

703 Juutinen, S., Virtanen, T., Kondratyev, V., Laurila, T., Linkosalmi, M., Mikola, J., Nyman, J.,  
704 Räsänen, A., Tuovinen, J-P., and Aurela, M.: Spatial variation and seasonal dynamics  
705 of leaf-area index in the arctic tundra – implications for linking ground observations  
706 and satellite images. *Environmental Research Letters* 12, doi.org/10.1088/1748-  
707 9326/aa7f85, 2017.

708 Kuhn, M. A., Varner, R. K., Bastviken, D., Crill, P., MacIntyre, S., Turetsky, M., Walter Anthony,  
709 K., McGuire, A. D., and Olefeldt, D.: BAWLD-CH<sub>4</sub>: a comprehensive dataset of  
710 methane fluxes from boreal and arctic ecosystems, *Earth Syst. Sci. Data*, 13, 5151–  
711 5189, <https://doi.org/10.5194/essd-13-5151-2021>, 2021.

712 Lau, M.C.Y., Stackhouse, B.T., Layton, A.C., Chauhan, A., Vishnivetskaya, T.A., Chourey, K.,  
713 Ronholm, J., Mykityczuk, N.C.S., Bennett, P.C., Lamarche-Gagnon, G., Burton, N.,  
714 Pollard, W.H., Omelon, C.R., Medvigy, D.M., Hettich, R.L., Pfiffner, S.M., Whyte,  
715 L.G., and Onstott, T.C.: An active atmospheric methane sink in high Arctic mineral  
716 cryosols. *The ISME Journal* 9, 1880–1891, doi:10.1038/ismej.2015.13, 2015.

717 Lafleur, P.M., Humphreys, E.R., St. Louis, V.L., Myklebust, M.C., Papakyriakou, T., Poissant, L.,  
718 Barker, J.D., Pilote, M., and Swystun, K.A.: Variation in Peak Growing Season Net  
719 Ecosystem Production Across the Canadian Arctic. *Environmental Science and*  
720 *Technology* 46, 7971–7977, doi.org/10.1021/es300500m, 2012.

721 Lara, M.J., McGuire, A.D., Euskirchen, E.S., Genet H., Yi, S., Rutter, R., Iversen, C., Sloan, V.,  
722 and Wullschleger, S.D.: Local-scale Arctic tundra heterogeneity affects regional-scale  
723 carbon dynamics- *Nature Communications* 11, 4925, doi:10.1038/s41467-020-18768-  
724 z, 2020.

725 Lohila, A., Aalto, T., Aurela, M., Hatakka, J., Tuovinen, J-P., Kilkki, J., Penttilä, T., Vuorenmaa, J.,  
726 Hänninen, P., Sutinen, R., Viisanen, Y., and Laurila, T.: Large contribution of boreal  
727 upland forest soils to a catchment-scale CH<sub>4</sub> balance in a wet year. *Geophysical*  
728 *Research Letters* 43, 2946–2953, doi.org/10.1002/2016GL067718, 2016.

729 Marushchak, M.E., Kiepe, I., Biasi, C., Elsakov, V., Friborg, T., Johansson, T., Soegaard, H.,  
730 Virtanen, T., and Martikainen, P.J.: Carbon dioxide balance of subarctic tundra from  
731 plot to regional scales. *Biogeosciences* 10, 437–452, doi:10.5194/bg-10-437-2013,  
732 2013.

733 McCalley, C.K., Woodcroft, B.J., Hodgkins, S.B., Wehr, R.A., Kim, E-H., Mondav, R., Crill, P.M.,  
734 Chanton, J.P., Rich, V.I., Tyson, G.W., and Saleska, S.R.: Methane dynamics  
735 regulated by microbial community response to permafrost thaw. *Nature* 514, 478–451,  
736 doi:10.1038/nature13798, 2014.

737 McFadden, J.P., Eugster, W., and Chapin, F.S., III: A regional study of the controls on water vapor  
738 and CO<sub>2</sub> exchange in arctic tundra. *Ecology* 84, 2762–2776, doi:10.1890/01-0444,  
739 2003.

740 McGuire, A. D., Christensen, T. R., Hayes, D., Heroult, A., Euskirchen, E., Kimball, J. S., Koven,  
741 C., Lafleur, P., Miller, P. A., Oechel, W., Peylin, P., Williams, M., and Yi, Y.: An  
742 assessment of the carbon balance of Arctic tundra: comparisons among observations,  
743 process models, and atmospheric inversions, *Biogeosciences*, 9, 3185–3204,  
744 <https://doi.org/10.5194/bg-9-3185-2012>, 2012.

745 McGuire, A.D., Lawrence, D.M., Koven, C., Clein, J.C., Burke, E., Chen, G., Jafarov, E.,  
746 MacDougall, A.H., Marchenko, S., Nicolsky, D., Peng, S., Rinke, A., Ciais, P.,  
747 Gouttevin, I., Hayes, D.J., Jin, D., Krinner, G., Moore, J.C., Romanovsky, V.,  
748 Schädel, C., Schaefer, K., Schuur, E.A.G., and Zhuang, Q.: Dependence of the  
749 evolution of carbon dynamics in the northern permafrost region on the trajectory of  
750 climate change, *PNAS* 115, 3882–3887, doi/10.1073/pnas.1719903115, 2018.

751 Mikola, J., Virtanen, T., Linkosalmi, M., Vähä, E., Nyman, J., Postanogova, O., Räsänen, A.,  
752 Kotze, D.J., Laurila, T., Juutinen, S., Kondratyev, V., and Aurela, M.: Spatial  
753 variation and linkages of soil and vegetation in the Siberian Arctic tundra – coupling  
754 field observations with remote sensing data. *Biogeosciences* 15, 2781–2801, 2018.

755 Oh, Y., Zhuang, Q., Liu, L., Welp, L.R., Lau, M.C.Y., Onstott, T.C., Medvigy, D., Bruhwiler, L.,  
756 Dlugokencky, E.J., Hugelius, G., D’Imperio, L., and Elberling, B. Reduced net

757 methane emissions due to microbial methane oxidation in a warmer Arctic. *Nature*  
758 *Climate Change* 10, 317–321, 2020.

759 St Pierre, K.A., Kortegaard Danielsen, B., Hermesdorf, L., D'Imperio, L., Lønsmann Iversen, L.,  
760 Elberling, B.: Drivers of net methane uptake across Greenlandic dry heath tundra  
761 landscapes. *Soil Biology and Biochemistry* 138: 107605,  
762 doi.org/10.1016/j.soilbio.2019.107605, 2019.

763 Räsänen, A., Manninen, T., Korhonen, M., Lohila, A., and Virtanen, T.: Predicting catchment-  
764 scale methane fluxes with multi-source remote sensing. *Landscape Ecology* 36, 1177–  
765 1195. <https://doi.org/10.1007/s10980-021-01194-x>. 2021.

766 Richardson, A.D.: Tracking seasonal rhythms of plants in diverse ecosystems with digital camera  
767 imagery. *New Phytologist* 222, 1742–1750, doi: 10.1111/nph.15591, 2019.

768 Sá, M.M.F., Schaefer, C.E.G.R., Loureiro, D.C., Simas, F.N.B., Alves, B.J.R., de Sá Mendonça, E.,  
769 Barretto de Figueiredo, E., La Scala, N., Panosso, A.R., Fluxes of CO<sub>2</sub>, CH<sub>4</sub>, and  
770 N<sub>2</sub>O in tundra-covered and Nothofagus forest soils in the Argentinian Patagonia,  
771 *Science of The Total Environment*, 659, 401-409,  
772 <https://doi.org/10.1016/j.scitotenv.2018.12.328>, 2019.

773 Saunio, M., Stavert, A.R., Poulter, B., Bousquet, P., Canadell, J.G., Jackson, R.B., Raymond, P.A.,  
774 Dlugokencky, E.J., Houweling, S., Patra, P.K. and Ciais, P.: The global methane  
775 budget 2000–2017. *Earth System Science Data*, 12, 1561-1623, 2020.

776 Shaver, G.R., Street, L.E., Rastetter, E.B., van Wijk, M.T., and Williams, M.: Functional  
777 convergence in regulation of net CO<sub>2</sub> flux in heterogeneous tundra landscapes in  
778 Alaska and Sweden. *Journal of Ecology* 95, 802–817, 2007.

779 Street, L.E., Shaver, G.R., Williams, M., and van Wijk, M.T.: What is the relationship between  
780 changes in canopy leaf area and changes in photosynthetic CO<sub>2</sub> flux in arctic  
781 ecosystems? *Journal of Ecology* 95, 139–150, 2007.



782 Ter Braak, C.J.F. and Šmilauer, P.: Canoco reference manual and user's guide: software for  
783 ordination (version 5.0). Microcomputer Power, Ithaca, NY, USA, 2012.

784 Treat, C.C., Marushchak, M.E., Voigt, C., Zhang, Y., Tan, Z., Zhuang, Q., Virtanen, T.A., Räsänen,  
785 A., Biasi, C., Hugelius, G., Kaverin, D., Miller, P.A., Stendel, M., Romanovsky, V.,  
786 Rivkin, F., Martikainen, P.J., and Shurpali, N.J. Tundra landscape heterogeneity, not  
787 interannual variability, controls the decadal regional carbon balance in the Western  
788 Russian Arctic. *Global Change Biology* 24, 5188–5204, doi: 10.1111/gcb.14421,  
789 2018.

790 Tuovinen, J-P., Aurela, M., Hatakka, J., Räsänen, A., Virtanen, T., Mikola, J., Ivakhov, V.,  
791 Kondratyev, V., and Laurila, T.: Interpreting eddy covariance data from  
792 heterogeneous Siberian tundra: land-cover-specific methane fluxes and spatial  
793 representativeness. *Biogeosciences* 16, 255–274, doi.org/10.5194/bg-16-255-2019,  
794 2019.

795 Uttal, T., Starkweather, S., Drummond, J. R., Vihma, T., Makshtas, A. P., Darby, L. S., Burkhart,  
796 J. F., Cox, C. J., Schmeisser, L. N., Haiden, T., Maturilli, M., Shupe, M. D., de Boer,  
797 G., Saha, A., Grachev, A. A., Crepinsek, S. M., Bruhwiler, L., Goodison, B.,  
798 McArthur, B., Walden, V. P., Dlugokencky, E. J., Persson, P. O. G., Lesins, G.,  
799 Laurila, T., Ogren, J. A., Stone, R., Long, C. N., Sharma, S., Massling, A., Turner,  
800 D. D., Stanitski, D. M., Asmi, E., Aurela, M., Skov, H., Eleftheriadis, K., Virkkula,  
801 A., Platt, A., Førland, E. J., Iijima, Y., Nielsen, I. E., Bergin, M. H., Candlish, L.,  
802 Zimov, N. S., Zimov, S. A., O'Neill, N. T., Fogal, P. F., Kivi, R., Konopleva-Akish,  
803 E. A., Verlinde, J., Kustov, V.Y., Vasel, B., Ivakhov, V.M., Viisanen, Y., and Intrieri,  
804 J. M.: International Arctic Systems for Observing the Atmosphere: An International  
805 Polar Year Legacy Consortium. *Bull. Am. Meteor. Soc.*, 97, 1033–  
806 1056. doi:10.1175/BAMS-D-14-00145.1, 2016.

807 Webb, E.E., Schuur, E.A.G., Natali, S.M., Oken, K.L., Bracho, R., Krapek, J.P., Risk, D., and  
808 Nickerson, N.R.: Increased wintertime CO<sub>2</sub> loss as a result of sustained tundra  
809 warming, *Journal of Geophysical Research Biogeosciences* 121, 249–265,  
810 doi:10.1002/2014JG002795, 2016.

811 Wickland, K.P., Jorgenson, M.T., Koch, J.C., Kanevskiy, M., and Striegl, R.G.: Carbon dioxide and  
812 methane flux in a dynamic Arctic tundra landscape: Decadal-scale impacts of ice  
813 wedge degradation and stabilization. *Geophysical Research Letters*, 47,  
814 e2020GL089894, doi:10.1029/2020GL089894, 2020.

815 van der Molen, M.K., van Huissteden, J., Parmentier, F.J.W., Petrescu, A.M.R., Dolman, A.J.,  
816 Maximov, T.C., Kononov, A.V., Karsanaev, S.V., and Suzdalov, D.A.: The growing  
817 season greenhouse gas balance of a continental tundra site in the Indigirka lowlands,  
818 NE Siberia. *Biogeosciences* 4, 985–1003, doi.org/10.5194/bg-4-985-2007, 2007.

819 Virkkala, A.-M., Virtanen, T., Lehtonen, A., Rinne, J., and Luoto, M.: The current state of CO<sub>2</sub> flux  
820 chamber studies in the Arctic tundra: A review. *Progress in Physical Geography*, 42,  
821 162–184, 2018.

822 Virkkala, et al.: Statistical upscaling of ecosystem CO<sub>2</sub> fluxes across the terrestrial tundra and  
823 boreal domain: regional patterns and uncertainties. *Global Change Biology*,  
824 doi:10.1111/GCB.15659, 2021.

825 Virtanen, T. and Ek, M.: The fragmented nature of tundra landscape. *International Journal of*  
826 *Applied Earth Observation and Geoinformation* 27, 4–12, 2014.

827 Zhang, W., Jansson, P-E., Sigsgaard, C., McConnell, A., Manon Jammet, M., Westergaard-Nielsen,  
828 A., Lund, M., Friborg, T., Michelsen, A., and Elberling, B.: Model-data fusion to  
829 assess year-round CO<sub>2</sub> fluxes for an arctic heath ecosystem in West Greenland  
830 (69°N). *Agricultural and Forest Meteorology* 272–273, 176–186, 2019.

831  
832

833 **Appendix A**

834

835



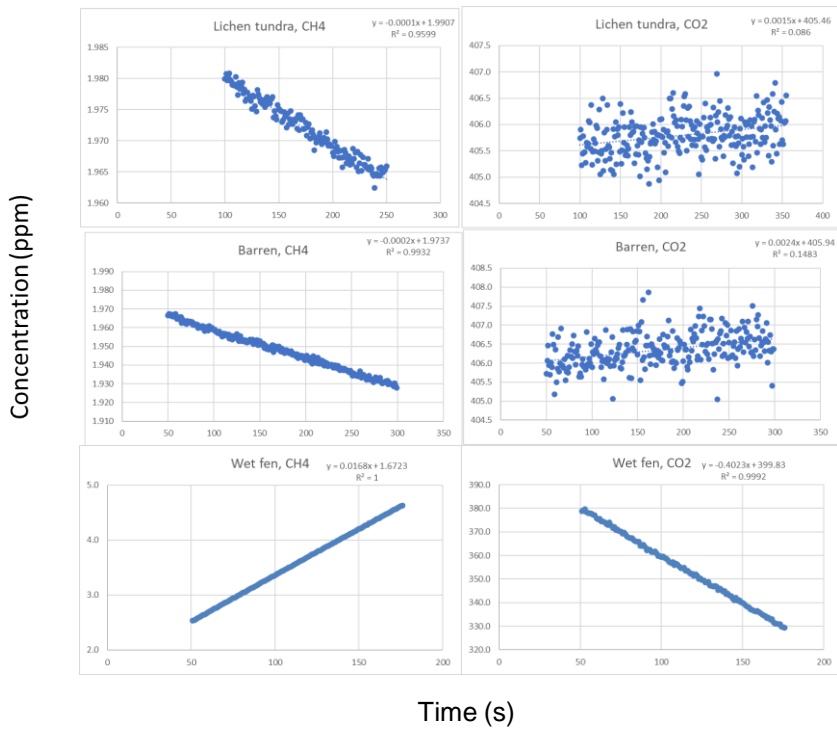
836

837 Fig. A1. Examples of the barren (left) and lichen tundra (right) plots with close views (bottom).  
838 Vegetation consists of lichens *Flavocetraria* sp., *Thamnolia* sp., *Alectoria* sp., dwarf-shrubs *Dryas*  
839 *octopetala*, *Vaccinium vitis-idaea*, *Cassiope tetragona*, and graminoids and forbs such as *Carex*  
840 *spp.* and *Polygonum viviparum*.

841

842

843

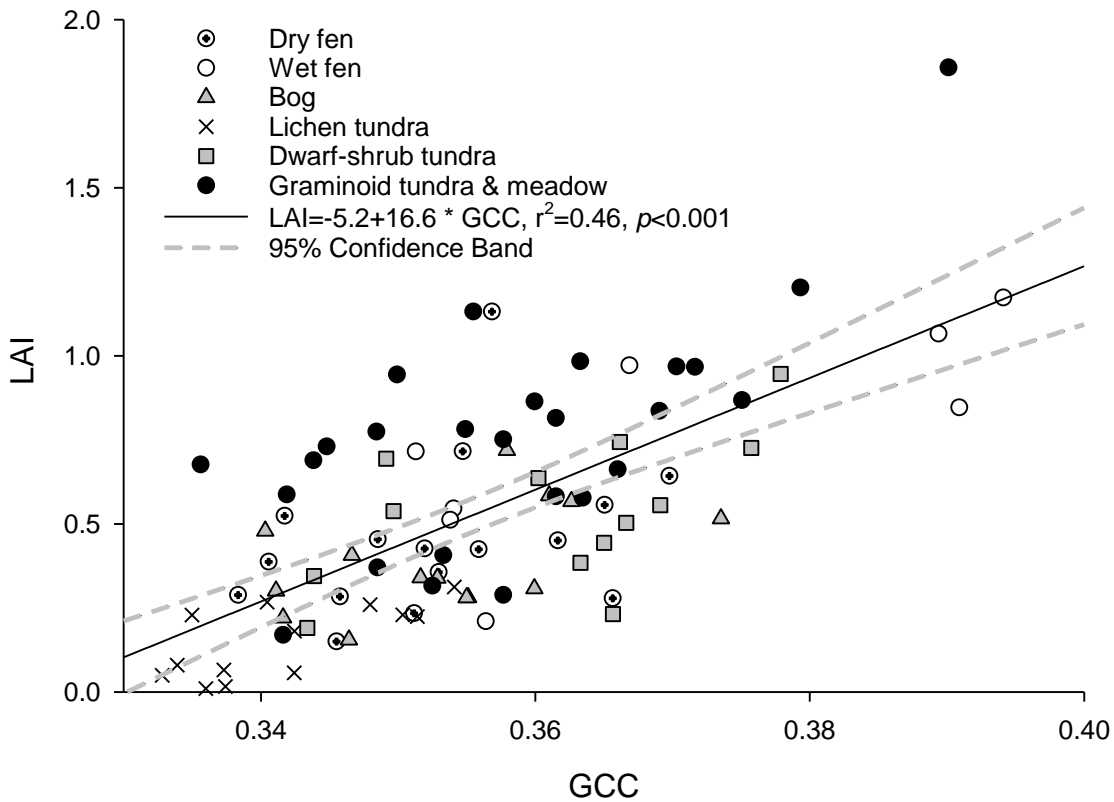


844

845 Fig.A2. Examples of gas concentrations in chambers measured using the LGR analyzer. The  
 846 examples represent lichen tundra, barren, and wet fen.

847

848



849

850 Figure A3. Relationship between GCC and vascular plant LAI in the harvested plots. LCTs are  
 851 indicated with symbols. In the LCT-specific regressions (not shown), the coefficient of  
 852 determination ( $R^2_{adj.}$ ) was lowest for dry fen (0.06) and highest for wet fen (0.54). Regression  
 853 slopes varied from 8.3 for dry fen to 17.8 for the combined graminoid tundra and meadow LCT.

854